Potential impact of carbonaceous aerosol on the Upper Troposphere and Lower Stratosphere (UTLS) and precipitation during Asian summer monsoon in a global model simulation

Suvarna Fadnavis[1], Gayatry Kalita[1], K. Ravi Kumar[1], Blaz Gasparini[2] and Jui-Lin Frank Li[3]

[1]Indian Institute of Tropical Meteorology, Pune, India

[2]Institute for Atmospheric and Climate Science, ETH Zürich, Switzerland

[3]Jet Propulsion Laboratory, California Institute of Technology, Pasadena, California

Abstract

Recent satellite observations show efficient vertical transport of Asian pollutants from the surface to the upper level anticyclone by deep monsoon convection. In this paper, we examine the transport of carbonaceous aerosols including Black Carbon (BC) and Organic Carbon (OC) into the monsoon anticyclone using of ECHAM6-HAM, a global aerosol climate model. Further, we investigate impacts of enhanced (doubled) carbonaceous aerosols emissions on the UTLS, underneath monsoon circulation and precipitation from sensitivity simulations.

These model simulations show that boundary layer aerosols are transported into the monsoon anticyclone by the strong monsoon convection from the Bay of Bengal, southern slopes of the Himalayas and the South China Sea. Doubling of emissions of BC and OC aerosols, each, over the South East Asia (10°S - 50°N; 65°E - 155°E) show that lofted aerosols enhance radiative heating rates (0.02-0.03 K/day) near the tropopause, produce significant warming (1K), and instability in the mid/upper troposphere. The enhanced carbonaceous aerosols alter aerosol Radiative Forcing (RF) at the surface by –4.74 W/m^2; at the Top Of the Atmosphere

(TOA) by +0.37 W/m^2 and in the atmosphere by +5.11 W/m^2 over the Asian summer monsoon region (20ºN - 40°N, 60ºE - 120°E). Atmospheric warming increases vertical velocities and thereby cloud ice in the upper troposphere. An anomalous warming over the Tibetan Plateau (TP) facilitates the relative strengthening of the monsoon Hadley circulation and increases moisture inflow by strengthening the cross-equatorial monsoon jet. This increases precipitation amounts over India and north east China.

Key words: Aerosol radiative forcing; Black Carbon and Organic Carbon aerosols; ECHAM6-HAM; Upper Troposphere and Lower Stratosphere (UTLS); Asian Tropopause Aerosol Layer (ATAL).

1. Introduction

South East Asia (10°S–50°N; 65°E–155°E) is one of the most fast-growing regions in terms of population and economy which contributes significantly to the emission of global aerosol particles (Ramanathan and Crutzen, 2003; Lin et al., 2013). India and China are the two main contributors in Asia (Carmichael et al., 2009; Lin et al., 2014; Butt et al., 2016). Black Carbon (BC) and Organic Carbon (OC) are the important aerosol species as they substantially contribute to the climate forcing (Penner et al., 1998; Chung and Seinfeld, 2002; Ramanathan and Carmichael, 2008; Hodnebrog et al., 2014), alter the energy balance in the atmosphere and the global water cycle (Solomon et al., 2007). Recent studies show that their impacts on local meteorology and monsoon circulation are large (Ackerman et al., 2000; Ramanathan et al., 2001a, 2001b; Lelieveld et al., 2001; Menon et al., 2002; Manoj et al., 2011). BC and OC together account for more than 60 % of the Aerosol Optical Depth (AOD) (Chin et al., 2009; Streets et al., 2009).

There is ever growing concern for rapidly increasing anthropogenic emissions of carbonaceous aerosols namely BC and OC. Global emissions of BC have almost doubled during the past century (Baron et al., 2009). Developing countries in Asia, e.g. India and China produce BC emissions at high growth rates. These countries together produced about 40% of total world BC emissions from combustion (Kopp and Mauzerall, 2010). The estimated growth of BC is 46 % (33% in OC) over China and 41% (35% in OC) over India during 2000 to 2010 (Lu et al., 2011). On a regional scale, their emissions are high over densely populated Indo-Gangetic Plains in India and eastern China (Kumar et al., 2011; Lelieveld, 2001; Gautam et al., 2011; Fadnavis et al., 2013; Zhang et al., 2015). Over the Asian region, (Indo-Gangetic Plains and north-eastern China) emission of OC is almost twice as that of BC (Fig. 1).

The majority of BC and OC aerosols are formed by incomplete combustion (Satheesh and Ramanathan; 2000; Carmichael et al., 2009). The important emission sources of BC aerosols are diesel vehicles, exhaust from coal-based power plants, exhaust from industries, forest fires and residential bio-fuel and fossil-fuel combustion. The OC aerosols are emitted from fossil fuel and biofuel burning and natural biogenic emissions. Biogenic carbonaceous aerosol are produced from of plant debris, pollen, fungal spores, and bacteria (Jacobson et al., 2000; Bond et al., 2004) and secondary organic aerosol from the oxidation of volatile organic compounds (VOCs) (Solomon et al., 2007).

Recent satellites, Cloud Aerosol Lidar and Infrared Path finder Satellite Observation (CALIPSO) (Vernier et al., 2011; Thomason and Vernier, 2013), Stratospheric Aerosol and Gas Experiment II (SAGE) (Thomason and Vernier, 2013) and Balloonsonde (Vernier, et al., 2015) observations show Asian Tropopause Aerosol Layer (ATAL) near the tropopause persisting during the monsoon season (June-September). Satellite observations reveal transport of trace gasses (CO, PAN, H_2O HCN) into the upper level monsoon anticyclone by deep monsoon convection (Park et al., 2009; Randel et al., 2010, Kunze et al.,2010; Ploeger et al., 2011; 2012; 2013; Fadnavis et al., 2014; 2015, Govardhan et al., 2017). Moreover, both back trajectory analysis based on CALIOP observations (Vernier et al., 2015) and modeling studies (Fadnavis et al., 2013) indicate that deep monsoon convection transports boundary layer aerosols into the UTLS. A Civil Aircraft for Regular Investigation of atmosphere Based on an Instrument Container (CARBIC) measurements show aerosols at the lower levels in the ATAL contain higher levels of carbonaceous and sulphate aerosols. The ratio of carbon to sulfur is ~4.0 with concentrations of carbon ~36 ng/m^3 and sulfur ~ 13 ng/m^3 in the Asian upper troposphere during August 2006, 2007 and 2008 (Vernier et al., 2015). Carbonaceous aerosols in the upper

troposphere lead to atmospheric heating due to their absorptive properties which may subsequently alter the atmospheric thermal structure and cloud amounts. Higher concentrations of carbonaceous aerosols in the ATAL may significantly alter thermal structure of the UTLS and therefore the underneath monsoon circulation (Meehl et al., 2008; Kloster et al., 2009). The ATAL may affect the Radiative Forcing (RF) regionally. Vernier et al., (2015) reported that the ATAL had exerted a short-term regional forcing at the top of the atmosphere ~ -0.1 W/m^2 during past two decades.

BC and OC aerosols absorb and scatter radiation, resulting in heating of the atmosphere and a layer of aerosols in the UTLS may reduce solar radiation reaching the Earth's surface (Penner et al., 1998). The global mean estimated cumulative (since 1970) BC radiative effect is +0.3 W/m^2 while OC emitted from fossil fuels is estimated to be -0.1 W/m^2 (Myhre et al., 2013). The presence of BC aerosols can change the sign of forcing from negative to positive (Haywood and Shine, 1997). Studies pertaining to BC/OC RF are sparse over the Indian region. Sreekanth et al., (2007) reported BC RF at the TOA +2.36 W/m^2 and -9.9 W/m^2 at the surface at Visakhapatnam (17.7ºN, 83.3ºE) during the monsoon season 2006. Babu et al., (2002) obtained BC RF +5 W/m^2 at the TOA and at the surface -23 W/m^2 at Bangalore (13ºN, 77ºE), during November-December 2001. Badarinath and Latha, (2006) reported BC RF of +9 W/m^2 at the TOA and -33 W/m^2 at the surface at Hyderabad (78ºE, 17ºN), India during January-May 2005.

Asian Summer Monsoon (ASM) has a major impact on agriculture, water resources, and economy and social life. Therefore it is important to study the impact of fast-growing Asian emission of carbonaceous aerosols on monsoon precipitation. However, there are a few studies reporting the impacts of carbonaceous aerosols on precipitation over India (Meehl et al., 2008; Wang et al., 2009; Ganguly et al., 2012) and China (Guo et al., 2013; 2015). Since convective

transport (during the monsoon season) inter-links tropospheric processes with the UTLS (Randel et al., 2010; Vogel et al., 2011, 2015; Fadnavis et al., 2013), it is essential to understand impacts of boundary layer emissions on the UTLS. To our knowledge, transport of carbonaceous aerosols from the boundary layer to upper troposphere, their impacts on the UTLS and connecting monsoon circulation are not explored in detail. In this study, we address the question of the impact of rapidly growing emissions of carbonaceous aerosols (BC and OC) on the thermal structure of the UTLS, monsoon transport processes and rainfall over India and China. We perform control and sensitivity simulations using the ECHAM6-HAM aerosol climate model. In sensitivity experiment, we have doubled anthropogenic emissions of BC and OC, each, over the South East Asia (10°S-50°N; 65°E-155°E). The paper is organized as follows; in Section 2 model simulations and satellite observations are described. The transport processes are discussed in Section 3. The impact of enhanced carbonaceous aerosols emissions on the UTLS and monsoon precipitation are described in Section 4, followed by conclusions given in Section 5.

2. Model simulations and satellite data analysis

2.1 Experimental setup and model simulations

The fully coupled aerosol-climate model ECHAM6-HAM (version echam6.1.0-ham2.1-moz0.8) used in this study comprises the general circulation model ECHAM6 (Stevens et al., 2013) coupled to the aerosol sub-module Hamburg Aerosol Model (HAM) (Stier et al., 2005, Zhang et al., 2012). HAM predicts the evolution of sulfate (SU), black carbon (BC), particulate organic matter (POM), sea salt (SS), and mineral dust (DU) aerosols. The size distribution of aerosol population being described by seven log-normal modes with prescribed variance as in the M7 aerosol module (Vignati et al., 2004; Stier et al., 2005; Zhang et al., 2012). Moreover, HAM

126 uses the two-moment cloud microphysics scheme in which the nucleation scavenging of aerosol
127 particles by acting as cloud condensation nuclei or ice nuclei, freezing and evaporation of cloud
128 droplets and melting and sublimation of ice crystals is treated explicitly (Lohmann et al., 2010,
129 Neubauer et al., 2014). The anthropogenic and fire emissions of SO_2, BC, and OC are based on
130 the AEROCOM-ACCMIP-II emission inventory. The anthropogenic emissions are based on
131 Lamarque et al., (2010). The biomass burning emissions are from GICC 1850 -1950 (Mieville et
132 al., 2010), RETRO 1960-1990 (Schultz et al., 2008) and GFED v2 (1997 - 2008) (van der Werf
133 et al., 2006). Biogenic emissions are derived from MEGAN (Guenther et al., 1995), and fossil
134 fuel sources are provided by the ACCMIP inventory (Lamarque et al., 2010). In the model,
135 biogenic OC is directly inserted via emissions. Secondary organic aerosol (SOA) emissions are
136 as described by Dentener et al. (2006). The emissions of sea salt (Guelle et al., 2001 and Stier et
137 al., 2005) and dust (Tegen et al., 2002; Cheng et al., 2008) are computed interactively.

138 The model simulations are performed at the spectral resolution of T63. This spectral
139 representation is associated with a horizontal resolution of 1.875° x 1.875° on a Gaussian grid and
140 a vertical resolution of 47 levels spanning from the surface up to 0.01 hPa. The simulations have
141 been carried out at a time step of 20 minutes. AMIP sea surface temperature (SST) and sea ice
142 cover (SIC) are used as lower boundary conditions. Note that our base year for aerosol and trace
143 gas emissions is 2000. Each simulation was performed for the 30 years from January 1979 to
144 December 2009. We analyze simulated data for 20 years (1989-2009) considering initial ten
145 years as spin-up time. Emissions are the same in each simulation, and meteorology varied
146 because of different monthly sea surface temperature (SST) and sea ice (SIC) data. The
147 interactive aerosols change the meteorology and feedback to aerosols variations Most of the
148 models underestimate BC and OC mass concentrations observed over Asia (Bond et al., 2013;

149 Butt et al., 2016; Winiger et al., 2016). Bond et al. (2013) have suggested that global atmospheric
150 absorption attributable to black carbon is too low in many models and should be increased by a
151 factor of three. Butt et al. (2016) obtained better predictions when residential carbonaceous
152 emissions were doubled. We performed control experiment (CTRL) with baseline emissions (for
153 the year 2000) and three sensitivity simulations for doubling of carbonaceous aerosols over the
154 Asian region; (1) Demiss in which emissions of BC and OC, both, are doubled, (2) emissions of
155 only BC aerosols are doubled in DBConly, and (3) simulation of doubling of only OC aerosols
156 refers to DOConly. We compare CTRL simulation with Demiss scenario to analyze the impacts
157 of doubled carbonaceous emissions (BC and OC together) on the UTLS and rainfall during ASM
158 season (June - September). We also provide contribution of BC and OC aerosols separately from
159 comparison of CTRL with DBConly and DOConly simulations.

160 **2.2 Satellite measurements**

161 **2.2.1 The Tropical Rainfall Measuring Mission (TRMM)**

162 The Tropical Rainfall Measuring Mission (TRMM) is a joint National Aeronautics and
163 Space Administration (NASA) - Japan Aerospace Exploration (JAXA) satellite mission to
164 monitor the tropical and subtropical precipitation and estimate its associated latent heat. TRMM
165 was launched in 1997 from Tanegashima space center in Japan. The rainfall measuring
166 instruments on the TRMM satellite include an electronically scanning radar Precipitation Radar
167 (PR), (operating at 13.6 GHz), TRMM microwave image (TMI), a 9 channel passive microwave
168 radiometer (which records radiation at the 10.65, 19.35, 37.0, 85.5 (V and H) and 21.3 (V) GHz),
169 and Visible and Infrared Scanner (VIRS) with five operating channels (Kummerow et al., 1998).
170 The 3B42 algorithm produces TRMM adjusted merged infrared precipitation rate and root mean
171 square (RMS) precipitation error estimates (Huffmen et al., 2007). The algorithm combines

multiple independent precipitation estimates from the TMI, Advanced Microwave Scanning Radiometer for Earth Observing Systems (AMSR-E), Special Sensor Microwave Imager (SSMI), Special Sensor Microwave Imager/Sounder (SSMIS), Advanced Microwave Sounding Unit (AMSU), Microwave Humidity Sounder (MHS), and microwave-adjusted merged geo-infrared (IR). The final 3B42 precipitation (in mm hr^{-1}) estimates have a 3-hourly temporal resolution and a 0.25-degree by 0.25-degree spatial resolution. TRMM precipitation can be obtained from https://disc2.gesdisc.eosdis.nasa.gov/data/TRMM_L3/TRMM_3B42.7/. 3-hourly precipitation data are averaged to obtain daily mean. Then, seasonal mean (June-September) is computed from daily mean data. Further, seasonal mean data is averaged for 20 years (1997-2016) to obtain climatology of the monsoon season.

2.2.2 CloudSat and Cloud-Aerosol Lidar Infrared Pathfinder Satellite Observations (CALIPSO)

Cloud–Aerosol Lidar and Infrared Pathfinder Satellite Observation (CALIPSO) and CloudSat are two A-Train constellation satellites, launched together in April 2006. They provide information related to the role of cloud and aerosol in the Earth's climate system and radiative imbalance of the atmosphere. The Cloud Profiling Radar (CPR) on board of CloudSat satellite is a 94-GHz nadir-looking radar which measures the power backscattered by clouds as a function of distance. It provides information on cloud abundance, distribution, structure, and radiative properties (Stephens et al., 2008). The Cloud-Aerosol Lidar with Orthogonal Polarization (CALIOP) is an elastically backscattered active polarization sensitive Lidar instrument onboard CALIPSO. The CALIOP transmit laser light simultaneously at 532 nm and 1064 nm at a pulse repetition rate 20.16Hz. The Lidar receiver subsystem measures backscatter intensity at 1064 nm and two orthogonally polarized components of 532 nm backscatter signal that provides the

information on the vertical distribution of aerosols and clouds, cloud particle phase, and classification of aerosol size (Winker et al., 2010; Powel et. al., 2013). In this study, we use Ice water content (IWC) dataset from the combined measurement of CloudSat and Calipso (2C-ICE_L3_V01) for the period 2007-2010. The 2C-ICE cloud product is an ice cloud retrieval derived from the combination of the CloudSat radar and CALIPSO Lidar, using a variational method for retrieving profiles of the IWC in ice clouds (Deng et al., 2013). The details of the data retrieval method are explained in Li et al., (2012). IWC data has been averaged for the monsoon season and period 2007-2010 to obtained seasonal climatology.

2.3 Comparison with in-situ measurements

We compare CTRL simulated BC concentrations with (1) aircraft measurements at Guwahati (26°11′N, 91°44′E) on 30August, 4 and 6 September 2009 from Rahul et al. (2014) and (2) Balloon borne measurements at Hyderabad (17º.48' N; 78º.40'E) (aethalometer installed on the hydrogen-inflated balloon) on 17 March 2010 from Babu et al., (2011). The model is not forced with meteorology therefore daily variations are not reproduced. Hence for comparison, monthly mean simulated BC concentrations are extracted at the grid centred at Guwahati and Hyderabad. Figure 2a-d shows the comparative analysis of model simulated BC and in-situ measurements. It can be seen that model underestimates BC emissions; therefore, we compare in-situ measurements with Demiss simulations, additionally. The profiles of BC concentration obtained from Demiss simulation show reasonable agreement with observations at Guwahati in the lower troposphere below 3km while differences are large between 3-6 km. Simulated BC profiles (CTRL and Demiss, both) show large differences with observations at Hyderabad (Fig.2d). These balloon-borne measurements show a variation of BC between 1000-10000 ng m^{-3} while simulated BC concentration varies between 3000-3 ng m^{-3}. The differences between in-situ

measurements (balloon borne and aircraft) and model simulations may be due to number of factors such as the uncertainty in BC emissions in the model's emission inventory, uncertainty in the model's transport processes, and it's coarse spatial grid (1.875° x 1.875°) compared to point measurement. Moreover, the meteorological conditions of each individual measurement day cannot be captured by monthly average values from the model output. The large differences at Hyderabad may be due to uncertainty in measurements due to attachment of aethalometer to the balloon. Although there are differences in the troposphere, Demiss simulations show reasonable agreement with measurements near the surface at Guwahati (Fig.2a-c) and Hyderabad (Fig. 2d). A similar agreement is also observed with observations near the surface (0-2km) at Kanpur (80º.20'E, 26º.26'N) (Tripathi et al., 2007). The BC concentrations at Kanpur obtained from Demiss simulations ~7.5 µg m^{-3} - 3 µg m^{-3} are comparable with observations ~8 µg m^{-3} - 4 µg m^{-3}.

Figures 2e and 2f show the vertical distribution of cloud ice obtained from CTRL simulation and climatology of the seasonal mean from combined measurement of CloudSat and CALIPSO (2C-ICE) (2007-2010) respectively, averaged for the monsoon season (June-September) and ASM region (60ºE - 110º E;15ºN - 40ºN). It can be seen that simulated (3 mg/kg -10 mg/kg) and observed cloud ice (5 mg kg^{-1} - 17 mg kg^{-1}), both, show high amounts in the upper troposphere (450 hPa - 200 hPa) over the ASM region. The model simulations show maximum (7 mg kg^{-1} - 10 mg kg^{-1}) at ~350 hPa - 250 hPa over 80ºE - 100ºE while satellite observations (12 mg kg^{-1} – 17 mg kg^{-1}) show it at ~450 hPa - 200 hPa over ~80ºE - 120ºE. These differences may be related to uncertainties in satellite observations (Deng et al., 2010) and model biases, e.g., the model does not consider large ice particles unlike the cloud ice measurement from CloudSat and CALIPSO. The total ice water mass estimate from 2C-ICE, combine

measurements from CALIPSO Lidar depolarization which is sensitive to small ice particle (i.e., cloud ice represented in GCMs) while CloudSat radar which is very sensitive to larger ice particles (i.e., precipitating ice or snow). In most global climate models including all the CMIP3 and most of the CMIP5, only small particles (i.e., cloud ice) are represented prognostically. The mass of large ice particles (about two-third of total ice) and their radiative effects, however, are not included (e.g., Li et al., 2012; 2013).

We compare simulated (CTRL) seasonal mean (June-September) precipitation with TRMM climatology (1997-2016). Figures 2g and 2h show the distribution of precipitation as obtained from CTRL simulation and TRMM respectively. It can be seen that general spatial pattern of precipitation simulated by the model is in good agreement with the TRMM. The model could reproduce high amounts of precipitation over the Bay of Bengal, the South China Sea, and the Western Ghats, in agreement with a numbers of past studies (Wang and Linho, 2002; Hirose and Nakamura, 2005; Xie et al., 2007; Takahashi, 2016). However, model underestimates the rainfall over northern India and the Western coast of India by ~ 2 mm/day - 10 mm/day and overestimates over the Tibetan Plateau (TP) and the South China Sea by ~5 mm/day - 12 mm/day. It may be related uncertainties in emissions, transport errors, and model coarse resolution.

3. Transportation of aerosol to the UTLS

Figure 3a depicts the vertical distribution of carbonaceous aerosols averaged over North India (75ºE - 100ºE; 25ºN - 45ºN) during the annual cycle as obtained from CTRL simulation. It shows elevated levels of aerosols (BC and OC together) from the surface to the tropopause during pre-monsoon (March-May) and monsoon seasons. It also shows a layer of carbonaceous

aerosols (~5 ng/m^3) in the upper troposphere ~170hPa - 100hPa. A layer of aerosols in the upper troposphere is also observed by satellite (SAGE II, CALIPSO) and Lidar measurements during the monsoon season (Vernier et al., 2011; Thomason and Vernier, 2013; Fadnavis et al. 2013; He et al., 2014). Over the TP this aerosol layer extends above the tropopause (18-19 km) (He et al., 2014).

A prominent feature in the UTLS over the ASM region during the summer season is a large anticyclone. Satellite observations show a persistent maximum in trace gases (CO, H_2O, PAN, HCN, CH_4, etc) (Li et al., 2005; Randel and Park 2006, Fu et al., 2006; Park et al., 2008; 2009, Randel et al., 2010; Fadnavis et al., 2013, 2014, 2015) and aerosols (Tobo et. al., 2007; Vernier et al., 2011; Thomason and Vernier, 2013; Yu et al., 2015) in the ASM anticyclone. Figure 3b exhibits the distribution of seasonal (June-September) mean carbonaceous aerosols (BC and OC together) from CTRL simulation in the anticyclone (~100 hPa). In agreement with previous studies (Tobo et al., 2007 Vernier et al., 2011), Fig. 3b also shows confinement of high carbonaceous aerosols concentration (~5.5 ng/m^3) within the anticyclone. The wind vector at 100 hPa depicts the extent of the anticyclone (20°E-120°E and 15°N-40°N).

Previous studies from model simulations and trajectory analysis show that rapid transport of trace gases and aerosols from Asian boundary layer into the anticyclone is closely linked with the deep ASM convection (Li et al, 2005; Randel and Park, 2006; Park et al., 2007; Park et al, 2009; Xiong et al., 2009; Fadnavis et al, 2013, 2014 , 2015). We plot longitude-pressure and latitude-pressure cross sections of carbonaceous aerosol from CTRL simulations to understand their transport. Figure 3c displays seasonal mean longitude-pressure variation of carbonaceous averaged over 15°N-35°N, along with wind vectors. It indicates that they are lifted up from the Bay of Bengal, Indo-Gangetic Plains (70ºE-90ºE) and South China Sea (110ºE-130ºE) into the

anticyclone increasing the aerosol concentration to 4-6 ng m^{-3} in the UTLS (above 200hPa) across 40°E-110°E. Transport from southern slopes of Himalaya is evident in Figs. 3d. The vertical distribution of both BC and OC show transport from above mentioned regions into the UTLS (Fig.S1). The amount of OC (3-4 ng m^{-3}) crossing the tropopause is higher than BC (0.8-1 ng m^{-3}). Figures 3e and 3f show the condensed cloud water (both liquid and ice). Its maxima point out areas of frequent deep convective activity over the Bay of Bengal and the South China Sea (Fig. 3e) and the southern flanks of the Himalayas (Fig. 3f). Thus transport of carbonaceous aerosols (seen in Figs. 3c and 3d) from these regions into the upper level anticyclone may be due to deep monsoon convection. Pollution transport (CO, HCN, NO_x, PAN) from the Asian region to the UTLS due to monsoon convection is also reported by Park et al. (2007), Randel et al. (2010), Fadnavis et al., (2014, 2015). Figures 3c and 3d show that a fraction of aerosols crosses the tropopause and enters into the lower stratosphere. It may be due to large scale upward motion within the anticyclone. Recently, trajectory analysis showed that air masses within the anticyclone are transported into the lower stratosphere in the northern subtropics (Garny and Randel, 2016). We analyze the vertical profile of anomalies of carbonaceous aerosols obtained from a difference between Demiss and CTRL simulations. Longitude-pressure and latitude-pressure cross sections of the anomalies are shown in Figs. 4a and 4b respectively. Enhanced anomalies are seen along the transport pathways, e.g., from the Bay of Bengal, the South China Sea and southern flanks of the Himalayas into the anticyclone. They show an enhancement of nearly 4 ng m^{-3} relative mass of aerosol near the tropopause and part of it (>2 ng m^{-3}) enters the lower stratosphere. Comparisons of DBConly and DOConly simulations with CTRL show anomalies in BC 3-5 ng m^{-3} and OC 8-12 ng m^{-3} in the lower stratosphere (not shown).

4. Impact of enhanced carbonaceous aerosols emissions

4.1 Impact on radiative forcing and heating rates

The convectively transported carbonaceous aerosols may alter RF, heating rates, temperature, and vertical velocities in the UTLS. The carbonaceous aerosol can affect the radiative energy balance of the atmosphere directly by scattering and absorbing solar radiation and indirectly by acting as cloud condensation nuclei (Rosenfield, 2000). Anomalies in aerosol RF estimated from Demiss, DBConly and DOConly simulation against CTRL are averaged for the monsoon season and ASM region (see Table-1). The seasonal mean anomaly of aerosol forcing for Demiss simulation is +0.37 W m^{-2} at the Top Of the Atmosphere (TOA) and -4.74W m^{-2} at the surface. The estimated aerosol forcing anomalies for DBConly (DOConly) simulation is +0.31 W m^{-2} (-0.51 W m^{-2}) at the TOA and -4.2 W m^{-2} (-1.9 W m^{-2}) at the surface. In comparison, AR5 assessment of global mean BC RF at the TOA is +0.4 W m^{-2} (Myhre et al., 2013). The atmospheric RF is computed from the difference between forcing at TOA and surface. It represents the energy trapped in the atmosphere due to the presence of higher amounts of carbonaceous aerosols. The resultant anomaly of atmospheric aerosol RF for Demiss is +5.11 W m^{-2}, and for DBConly (DOConly) +4.52 W m^{-2} (+1.45 W m^{-2}). Table-1 indicates that among the carbonaceous aerosols, the major contribution in enhancing atmospheric RF is due to BC aerosols although emission of OC higher than BC aerosols over Asia. This may be due to scattering and absorbing property of OC aerosols. From athelometer observations, Sreekanth et al., (2007) reported BC RF at the TOA +2.36 W/m^2 and -9.9 W/m^2 at the surface at Visakhapatnam (17.7ºN, 83.3ºE) during the monsoon season of the year 2006. These values are higher than anomalies of BC RF (DBConly-CTRL) (TOA +1.3W/m^2 and surface -5.0W/m^2) obtained at the grid centred at Visakhapatnam. These differences may be due to a comparison of

point observations at Visakhapatnam with model output extracted over a grid (1.875°x1.875°) centred at the same location. Also, BC aerosols are underestimated in the model (Fig.2a-c). Pan et al (2015) has shown model simulations with AEROCOM-ACCMIP-II emissions underestimate AOD over south Asia (15 to 44 %) in comparison with Multi-angle Imaging Spectro Radiometer observations.

The resulting short-wave plus long-wave atmospheric forcing due to doubled carbonaceous aerosols will translate to a significant atmospheric heating (Babu et al., 2002). We obtain anomalies in total Heating Rates (HR) due to carbonaceous aerosols (Demiss - CTRL). Figures 4c and 4d show longitude-pressure (averaged for 15ºN-35ºN) and latitude-pressure (averaged for 80ºE-110ºE), cross sections of HR anomalies during the monsoon season. Enhanced carbonaceous aerosols emissions increase HR near the surface over the Indo-Gangetic Plains, southern slopes of the Himalayas and south China. High emissions from these regions cause anomalous heating (0.08 K/day) in the lower troposphere (1000 hPa - 600 hPa). Positive anomalies of HR can be seen along the pathway through which carbonaceous aerosols are transported into the anticyclone. The carbonaceous aerosols have increased HR by ~0.02 K/day - 0.03 K/day near the tropopause in the AMS region in comparison with CTRL simulations (0.006 K/day - 0.01 K/day). FigureS2 exhibits latitude-pressure cross section of HR anomalies for DBConly and DOConly simulations. It can be seen that in transport pathways, anomalies of HR for DBConly simulation are higher than DOConly. This may be attributed to the high absorbing property of BC than OC although emissions of OC aerosols are higher than BC over Asia. Radiative heating of the tropopause region increases the vertical motion and transport into the lower stratosphere (Gettelman et al., 2004). Carbonaceous aerosols enhancement (> 2 ng/m^3) in

355 the lower stratosphere seen in Figs. 4a and 4b is due to increase in vertical motion in response to
356 enhanced aerosol HR. This indicates that aerosols induce positive feedback in vertical transport.

357 **4.2 Impact on temperature, circulation and precipitation**

358 Further, we analyze changes in temperature induced by doubled carbonaceous aerosol
359 emissions. Figures 4e and 4f show the longitude-pressure (averaged over 15ºN - 35ºN) and
360 latitude-pressure (averaged over 80°E - 110°E) cross sections of temperature anomalies. These
361 aerosols induce significant warming in the mid-troposphere (500 hPa -300 hPa) over the ASM
362 region and an anomalous warm core (warming ~1K) in the mid-upper troposphere (~400 hPa-
363 300 hPa) over the TP (Fig. 4f). This warming may be due to heating by aerosol and water vapour
364 together. The aerosol induced warming may enhance water vapour transport in the mid/upper
365 troposphere (discussed in section 4.3) in response to dynamical changes. The enhanced water
366 vapour would contribute additionally to this warming and provide positive feedback (Fig 7 a-b).
367 The warming over TP in response to doubling of BC (DBConly) and OC (DOConly) aerosols
368 individually is shown in FigS3. Warming due to BC aerosols is ~0.3-1.2K over the TP while OC
369 aerosols show cooling (-0.3K) over central TP and warming (+0.6K) over northern TP. The
370 warm core over the TP plays an important role in enhancing the ASM circulation (Flohn 1957;
371 Yanai et al., 1992; Meehl, 1994; Li and Yanai, 1996; Wu and Zhang, 1998) (discussed later in
372 this section). Figure 4e shows cooling near the tropopause in the anticyclone with a small patch
373 of positive anomalies over the TP (80º-100°E). During the monsoon season, cold temperatures in
374 the UTLS persist the over warm mid-troposphere (Randel and Park 2006; Park et al., 2007). Our
375 model simulations show that doubling of carbonaceous aerosol emissions amplifies the mid-
376 tropospheric warming and cooling near the tropopause. The mid-upper tropospheric warming
377 would enhance convective instability (Defouw, 1970). The strong negative anomalies in Brunt–

Väisälä frequency (an indication of strong convective instability) in the mid-upper troposphere (300 hPa - 200 hPa) confirm (Fig. 5a) positive feedback between warming and convective instability in the mid-upper troposphere.

During Northern hemispheric summer, heating over the TP maintains a large-scale thermally driven vertical circulation (Yanai et al., 1992). The analysis of simulated vertical velocities shows that carbonaceous aerosols induce positive anomalies over the southern TP and Indo-Gangetic plains (Figs 5b and 5c). Thus carbonaceous aerosols amplify warming (Fig. 4e and Fig. 4f) and enhance ascending motion over these regions. Previous studies (Rajagopalan and Molnar, 2013, Vinoj et al., 2014) have reported that the warm ascending air above the TP gradually spreads southward and descends over the northern Indian Ocean. The south-westerly winds at the surface, on the other hand, complete the monsoon Hadley cell. This local circulation system releases latent heat and further maintains the Tibetan warm core. Thus heating over the TP leads to increased Indian summer monsoon rainfall by enhancing the cross-equatorial circulation and concurrently strengthening both the Somali Jet (low level Jet) and the westerly winds that bring rainfall to India. Goswami et al., (1999) also reported that there is a strong correlation between monsoon Hadley circulation and precipitation. Figure 5d shows that carbonaceous aerosols strengthen the monsoon Hadley circulation, ascending motion over 10ºN - 20ºN and descending over 0º-10ºS. These aerosols reinforce low-level monsoon jet (850hPa) (seen in Fig. 5e and also Fig.5d) and outgoing long-wave radiation (Fig. 5e). Figure 5e show enhanced convection (negative anomalies in OLR) induced by the carbonaceous aerosols over the Arabian Sea, Bay of Bengal, a majority of the Indian subcontinent, Myanmar and East China region.

The carbonaceous aerosols also indirectly affect precipitation processes by altering the CCN and Cloud Droplet Number Concentration (CDNC) (Rosenfeld et al., 2002). In our model simulations, doubling of carbonaceous aerosols and related indirect effect result in enhancement of CDNC (8-12 mg^{-1}) and cloud water (5-20 $\mu g\ m^{-3}$) in the region of strong convection (The Bay of Bengal, southern slopes of the Himalayas and South China Sea) in the lower troposphere (Fig.6a-d).

Figures 4-6 suggest that enhanced emissions of carbonaceous aerosols increase the HR, and amplify warm anomalies in the middle troposphere and cold anomalies near the tropopause. Aerosol induced warming elicits enhancement in vertical velocities. These aerosols induce an anomalous warming over the TP which in turn strengthens the monsoon Hadley circulation, low level monsoon jet and convection over the Indian subcontinent and East China. Previous studies (Meehl et al., 1994; Krishnamurthy and Achuthavarier, 2012) have explained the mechanism of strengthening of the monsoon Hadley circulation facilitates enhance precipitation over the Indian region. Consequently, aerosol (carbonaceous) induced precipitation anomalies are positive over the Indian region (1 mm day^{-1} - 4 mm day^{-1}) (Fig. 7a). Strong positive anomalies (2 mm day^{-1} - 4 mm day^{-1}) are located over North India, the Bay of Bengal, Western coast of India and foothills of Himalaya. There is an enhancement in precipitation over North east China (0.2 mm day^{-1} - 2 mm day^{-1}) and some parts of central and south China (0.2 mm day^{-1} - 1 mm day^{-1}). We show anomalies in precipitation obtained from DBConly and DOConly with respect to CTRL in Figs. 7b-c. These figures show that BC aerosols induce positive precipitation anomalies (~1-5 mm day^{-1}) over the Indian region by strengthening of monsoon Hadley circulation (Fig.S4a) while OC aerosols elicit negative precipitation anomalies over India (-1mm day^{-1} - -5 mm day^{-1}), north eastern China (0 - -1mm day^{-1}) by producing subsidence over these regions (Fig. S4b). In

agreement with the present study, aerosol-climate modeling studies by Wang et al., (2004, 2007) also show enhancement in precipitation over India due to black carbon direct RF. Increase in the Indian summer monsoon precipitation due to the loading of absorbing aerosol (BC and dust) has been reported in the past (Lau and Kim., 2006; Vinoj et al., 2014; Fadnavis et al., 2016). In the current study, simulations are performed with prescribed SSTs. In the model setup, interactive aerosols change the meteorology and feedback to aerosols variations. Other model studies using prescribed SSTs (Chung et al., 2002; Menon et al., 2002; Lau and Kim, 2006) also show an increase in precipitation over India due to black carbon aerosols. These model simulations did not take into account aerosol feedback with SSTs, unlike coupled atmosphere-ocean general circulation model. However, ocean-atmosphere coupled models often need multi-century simulations to take into account slow response of SSTs (Danabasoglu and Gent, 2009). The coupled atmosphere slab ocean model by Ganguly et al. (2012) show a mix response of precipitation distribution on climate scale. It shows a reduction in precipitation over the western coastline of the Indian peninsula and an increase over north western part of Indian subcontinent. Reduction in precipitation is attributed to anthropogenic aerosols from Asia and remote locations. These differences are due to different model-set up; present study gives an impact of doubled Asian carbonaceous aerosol emissions using aerosol-atmosphere-climate model. On the other hand, Ganguly et al. (2012) show responses of all anthropogenic and biomass burning aerosols in the context of climatic change (pre-industrial and present day) accounting also the slow response of SSTs.

4.3 Impact on water vapour and cloud ice

Recently from satellite observations, Park et al., (2007) have shown that water vapour in the upper troposphere (~216 hPa) varies coherently with deep monsoon convection both

temporally and spatially. Transport of high water vapour in the UTLS by the monsoon convection has been reported in the past (Gettelman et al., 2004; Dessler and Sherwood, 2004; Fu et al., 2006; Randel and Park, 2006, Braesicke et al., 2011; Ploeger et al., 2013). We analyze the difference in water vapour anomalies (Demiss - CTRL) to understand the impact of doubled Asian carbonaceous aerosol emissions on the transport of water vapour in the UTLS. Figures 8a and 8b show an increase in water vapour in the upper troposphere and lower stratosphere 3% - 15% (~0.1 ppmv - 20 ppmv). Water vapour anomalies 10 % - 15% (~8 ppmv - 20 ppmv) are seen near 200 hPa and 1 % - 5% (~0.1 ppmv - 0.8 ppmv) near the tropopause. Fadnavis et al. (2013) reported an increase in water vapour (~ 0.1 ppmv - 10 ppmv) in the UTLS in response to the increasing aerosols which are in agreement with the current study. In the past, Gettleman et al. (2004), Fu et al. (2006), Fadnavis et al., (2013), Garny and Randel (2016) also reported transport of water vapour above the tropopause into the lower stratosphere during the monsoon season. Enhanced aerosol emissions increase water vapour transport into the lower stratosphere by enhancing HRs, mid/upper tropospheric warming, and vertical velocities. These elevated levels of water vapour will provide positive feedback by intensifying the HRs.

In addition to thermal and dynamical impact, aerosols in the UTLS also largely influence the formation and microphysical properties of cirrus clouds. Cirrus clouds have a great impact on radiation and intensity of the large-scale tropical circulation (Randall et al., 1989; Ramaswamy and Ramanathan, 1989; Liu et al., 2003). Figures 8c –8f show longitude-pressure and latitude-pressure cross sections of anomalies of cloud ice and Ice Crystal Number Concentration (ICNC). These figures show enhancement of anomalies of cloud ice (by 0.4µg m^{-3} - 2 µg m^{-3}) and ICNC (by 0.02 mg^{-1} - 0.05 mg^{-1}) occurrence in the upper troposphere (350 hPa - 100 hPa). Maximum increase (cloud ice by 2 µg/m^3, ICNC by 0.05 mg^{-1}), is seen in the 80°E -90°E, 20ºN - 30ºN

where stronger upwelling motion prevails (Figs. 8e and 8f). A fraction of positive anomalies of ICNC is seen near the tropopause indicating entrainment into the lower stratosphere. Positive anomalies in cloud ice and ICNC (in the upper troposphere) are due to enhancement in ASM deep convection (increase in heating rates, mid/upper tropospheric temperature, vertical velocity, and monsoon Hadley circulation) induced by the doubling of carbonaceous aerosols emissions.

5. Summary and conclusions

In this paper, we investigated impacts of enhanced Asian (65°E - 155°E; 10°S - 50°N) carbonaceous aerosols on the UTLS, underneath monsoon circulation and precipitation over India and China using a state of the art aerosol-climate model. We performed sensitivity experiments for doubling of carbonaceous aerosol emission over the Asian region.

To validate the model simulations, we compare simulated BC vertical profile with observations from aircraft measurements at Guwahati (26°11′N, 91°44′E) India during August-September 2009 and athelometer launched on Balloonsonde at Hyderabad (78ºE, 17ºN) on 17 March 2010 (pre-monsoon season); seasonal mean of simulated cloud ice content with climatology of combined measurements from CloudSat and CALIPSO (2007-2010); and simulated precipitation with climatology of TRMM observations (1997-2016). The aircraft measurements show reasonable agreement with BC concentrations obtained from doubling of carbonaceous aerosol simulation (Demiss) in the lower troposphere. In the troposphere, the difference between aircraft measurements and simulated BC vary with altitude. Balloonsonde measurements at Hyderabad show large differences with Demiss simulations in the troposphere. The spatial patterns of the simulated season mean (June - September) precipitation are comparable with climatology of TRMM precipitation (1997-2016) and cloud ice with combined measurements from CloudSat and CALIOP (2007-2010) respectively. Simulated cloud ice is

492 underestimated 2 mg kg^{-1}- 7 mg kg^{-1} in the UTLS (60ºE - 120°E; 15ºN - 40°N) during the
493 summer monsoon season.

494 Our model simulations show that monsoon convection over the Bay of Bengal, the South
495 China Sea and Southern flanks of the Himalayas transport Asian carbonaceous aerosol into the
496 UTLS. A persistent maximum of carbonaceous aerosols is seen within the anticyclone during the
497 ASM season, and a fraction of these aerosols enter the lower stratosphere. Doubling emissions of
498 carbonaceous aerosol over the Asian region leads to their enhancement (by 4-6 ng m^{-3}) in the
499 UTLS. They alter aerosol RF at the surface by -4.74 W m^{-2}; at the TOA by +0.37 W m^{-2} and in
500 the atmosphere by +5.11 W m^{-2}. Positive anomalies of heating rates are seen along the pathway
501 through which aerosols are transported into the anticyclone. These carbonaceous aerosols
502 increase heating rates in the anticyclone (~100 hPa) by 0.02 K day^{-1} - 0.03 K day^{-1}. They induce
503 significant warming (temperature increases by 1 K) in the mid/upper troposphere over the ASM
504 region. An anomalous in-atmospheric warming enhances vertical velocities and thereby cloud ice
505 (2 mg m^{-3}), ICNC (0.05 mg^{-1}). A significant increase in water vapour transport in the upper
506 troposphere 10-15% (0.5-10 ppmv) and 1-5 % (0.1 ppmv - 0.5 ppmv) near the tropopause is
507 apparently related to the mid/upper tropospheric warming. Doubling of carbonaceous aerosols
508 emissions enhance warming over the TP (~1K) and cold anomalies near the tropopause. The
509 warming over TP may be partially due to heating by water vapour creating a positive feedback.
510 The enhanced carbonaceous aerosols strengthen the monsoon Hadley circulation by intensifying
511 warming over TP. They strengthen the low level monsoon jet, convection and elicit precipitation
512 enhancement over India (1-4 mm/day) and eastern China (0.2 mm day^{-1}- 2 mm day^{-1}). In
513 agreement with the present study, aerosol-climate modeling studies by Wang et al., (2004, 2007)
514 also show enhancement in Indian summer monsoon precipitation due to black carbon direct RF.

The experiments with doubling of BC only (DBConly) and OC only (DOConly) aerosols indicate that the HRs due to BC is higher that of OC aerosols along the transport path ways (the Bay of Bengal and southern slopes of the Himalayas). BC aerosols induce anomalous warming over the TP and enhance positive precipitation anomalies (~1-5 mm day^{-1}) over the Indian region by strengthening of monsoon Hadley circulation. While, OC aerosols produce cooling over central TP and elicit negative precipitation anomalies over India (-1mm day^{-1} - -5 mm day^{-1}) and north eastern China (0 - -1mm $day^{-1)}$ by producing subsidence over these regions.

In the current study, simulations are performed with enhanced Asian carbonaceous aerosols and prescribed SSTs where interactive aerosols change the meteorology and feedback to aerosols variations. Other modeling studies using prescribed SSTs and increase in global BC emissions also show an increase in precipitation over India (Chung et al., 2002; Menon et al., 2002; Lau et al., 2006). Observational evidence also shows that heavy loading of absorbing aerosols (BC and Dust) over the Indian subcontinent facilitate the enhancement of monsoon rainfall over India (Lau and Kim, 2006; Vinoj et al., 2014).

We note that a realistic future emission scenario also includes the increasing emissions of sulfate aerosols and the response of climate and circulation to increasing CO_2 concentrations, which might interplay with the presented results and lead to different dynamical and climatic responses. Moreover, in future, we propose to re-evaluate the studies by using the regional model with a better resolution of the complex orography over Himalayas/TP, etc. Notwithstanding this, the work provides valuable insight into the influence of growing Asian carbonaceous aerosols emissions on the UTLS, connecting monsoon processes and precipitation in the Asian summer monsoon region.

Acknowledgement: Authors acknowledges with gratitude the High Power Computing Centre (HPC) in IITM, Pune, India, for providing computer resources and anonymous reviewers for valuable suggestions.

References:

Ackerman, A. S., Toon, O.B., Stevens, D.E., Heymsfield, A.J., Ramanathan,V., Welton,E,J.: Reduction of tropical cloudiness by soot, Science, 288,1042-1047, doi: 10.1126/science.288.5468.1042, 2000.

Babu, S. S., S. K. Satheesh, and K. K. Moorthy.: Aerosol radiative forcing due to enhanced black carbon at an urban site in India, Geophys. Res. Lett., 29, 1880, doi:10.1029/2002GL015826, 2002.

Babu, S. S., K. K. Moorthy, R. K. Manchanda, P. R. Sinha, S. K. Satheesh, D. P. Vajja, S. Srinivasan, V. H. A. Kumar.: Free tropospheric black carbon aerosol measurements using high altitude balloon: Do BC layers build "their own homes" up in the atmosphere?, Geophys. Res. Lett., 38, L08803, doi:10.1029/2011GL046654, 2011.

Badarinath, K. V. S. and Latha, M. K., Direct radiative forcing from black carbon aerosols over urban environment, Advances in Space Research, Volume 37, Issue 12, p. 2183-2188, 10.1016/j.asr.2005.10.034, 2006.

Baron, R.E., Montgomery, W.D., Tuladhar, S.D.,. An Analysis of Black Carbon Mitigation as a Response to Climate Change, http://fixtheclimate.com/component-1/the-result-prioritization/, accessed in February 2010, 2009.

Bond, T. C., Streets, D. G., Yarber, K. F., Nelson, S. M., Woo, J.-H., and Klimont, Z.: A technology-based global inventory of black and organic carbon emissions from combustion, J. Geophys. Res., 109, D14203, doi:10.1029/2003JD003697, 2004.

Bond, T.C., S. J. Doherty, D. W. Fahey, P. M. Forster,T. Berntsen, B. J. DeAngelo, M. G. Flanner, S. Ghan, B. Kärcher, D. Koch, S. Kinne, Y. Kondo, P. K. Quinn, M. C. Sarofim, M. G. Schultz, M. Schulz, C. Venkataraman, H. Zhang, S. Zhang, N. Bellouin, S. K. Guttikunda, P. K. Hopke, M. Z. Jacobson, J. W. Kaiser, Z. Klimont, U. Lohmann, J. P. Schwarz, D. Shindell, T. Storelvmo, S. G. Warren, and C. S. Zender.: Bounding the role of black carbon in the climate system: A scientific assessment, Journal Of Geophysical Research: Atmospheres, Vol. 118, 5380–5552, doi:10.1002/jgrd.50171, 2013.

Braesicke, P., O. J. Smith, P. Telford, and J. A. Pyle.:Ozone concentration changes in the Asian summer monsoon anticyclone and lower stratospheric water vapour: An idealised model study, Geophys. Res. Lett., 38, L03810, doi:10.1029/2010GL046228, 2011.

Butt, E. W. Rap A., Schmidt A., Scott C. E., Pringle K. J., Reddington1 C. L., Richards N. A. D., Woodhouse M. T., Ramirez-Villegas J., Yang H., Vakkari V., Stone E. A., Rupakheti M., Praveen P. S., van Zyl P. G., Beukes J. P., Josipovic M., Mitchell E. J. S., Sallu S. M., Forster P. M., and Spracklen D. V.: The impact of residential combustion emissions on atmospheric aerosol, human health, and climate, Atmos. Chem. Phys., 16, 873–905, doi:10.5194/acp-16-873-2016, 2016.

Carmichael, G. H., Bhupesh Adhikary,Sarika Kulkarni,Alessio D'Allura,Youhua Tang,David Streets,Qiang Zhang,TamI C. Bond, Veerabhadran Ramanathan, Aditsuda Jamroensan, and Pallavi Marrapu, Asian Aerosols: Current and Year 2030 Distributions and Implications to Human Health and Regional Climate Change,Environ. Sci. Technol., 43, 5811–5817, doi:10.1021/es8036803, 2009.

Cheng, T., Y. Peng, J. Feichter, and I. Tegen.: An Improvement on the dust emission scheme in the global aerosol-climate model ECHAM5-HAM, Atmos. Chem. Phys., 8, 1105-1117, doi:10.5194/acp-8-1105-2008, 2008.

Chin, M., Diehl, T., Dubovik, O., Eck, T. F., Holben, B. N., Sinyuk, A., and Streets, D. G.: Light absorption by pollution, dust, and biomass burning aerosols: a global model study and evaluation with AERONET measurements, Ann. Geophys., 27, 3439–3464, doi:10.5194/angeo-27-3439-2009, 2009.

Chung, S. H., and J. H. Seinfeld.: Global distribution and climate forcing of carbonaceous aerosols, J. Geophys. Res., 107(D19), 4407, doi:10.1029/2001JD001397, 2002.

Danabasoglu, G., and P. Gent Equilibrium climate sensitivity: Isit accurate to use a slab ocean model?, J. Clim., 22, 2494–2499,doi:10.1175/2008JCLI2596.1, 2009.

Defouw, R.J., Thermal-Convective Instability, Astrophysical Journal, 160,659-669, 1970.

Deng, M., G. G. Mace, Z. Wang, and H. Okamoto.: Tropical Composition, Cloud and Climate Coupling Experiment validation for cirrus cloud profiling retrieval using CloudSat radar and CALIPSO lidar, J. Geophys. Res., 115, D00J15, doi:10.1029/2009JD013104, 2010.

Deng, M., G. G. Mace, Z. Wang, and Lawsan, R. P.: Evaluation of Several A-Train Ice Cloud Retrieval Products with In Situ Measurements Collected during the SPARTICUS Campaign, Journal Of Applied Meteorology And Climatology, 52, 1014-1030, doi: 10.1175/JAMC-D-12-054.1, 2013.

612 Dentener, F., Kinne,S., Bond,T., Boucher,O., Cofala, J., Generoso, S., Ginoux, P., Gong,S.,.
613 Hoelzemann, J., Ito,A., Marelli,L., Penner, J., Putaud, J.P., Textor, C., Schulz, M.,
614 G.V.D., Werf, Wilson J.: Emissions Of primary aerosol and precursor gases in the years
615 2000 and 1750 prescribed data -sets for AeroCom, Atmos. Chem. Phys., 6, 4321-4344,
616 doi:10.5194/acp-6-4321-2006, 2006.
617 Dessler, A. E., and S. C. Sherwood.: Effect of convection on the summertime extratropical lower
618 stratosphere, J. Geophys. Res., 109, D23301, doi:10.1029/2004JD005209, 2004.
619 Fadnavis, S., Semeniuk, K., Pozzoli, L., Schultz, M. G., Ghude, S. D., Das, S., and Kakatkar,
620 R.: Transport of aerosols into the UTLS and their impact on the Asian monsoon region
621 as seen in a global model simulation, Atmos. Chem. Phys., 13, 8771–8786,
622 doi:10.5194/acp-13-8771-2013, 2013.
623 Fadnavis, S., Schultz, M. G., Semeniuk, K., Mahajan, A. S., Pozzoli, L., Sonbawne, S., Ghude,
624 S. D., Kiefer, M., and Eckert, E.: Trends in peroxyacetyl nitrate (PAN) in the upper
625 troposphere and lower stratosphere over southern Asia during the summer monsoon
626 season: regional impacts, Atmos. Chem. Phys., 14, 12725–12743, doi:10.5194/acp-14-
627 12725-2014, 2014.
628 Fadnavis, S., Semeniuk, K., Schultz, M. G., Kiefer, M., Mahajan, A., Pozzoli, L., and
629 Sonbawane, S.: Transport pathways of peroxyacetyl nitrate in the upper troposphere and
630 lower stratosphere from different monsoon systems during the summer monsoon season.
631 Atmos. Chem. Phys., 15, 11477-11499, doi:10.5194/acp-15-11477-2015, 2015.
632 Fadnavis, S.; Roy, Chaitri; Sabin, T. P.; Ayantika, D. C.; Ashok, K.: Potential modulations of
633 pre-monsoon aerosols during El Niño: impact on Indian summer monsoon, Clim.Dyn,1-
634 12,doi: 10.1007/s00382-016-3451-6, 2016.
635 Flohn, H.: Large-scale aspects of the summer monsoon in South and East Asia, J. Meteor. Soc.
636 Japan, 75, 180–186, doi: 551.553.21:551.589.5, 1957.
638 Fu, R., Hu, Y., Wright, J. S., Jiang, J. H., Dickinson, R. E., Chen, M., Filipiak, M., Read,W.
639 G.,Waters, J.W., and Wu, D. L.: Short circuit of water vapour and polluted air to the
640 global stratosphere by convective transport over the Tibetan Plateau, P. Natl. Acad. Sci.
641 USA, 103, 5664–5669, doi: 10.1073/pnas.0601584103, 2006.

642 Ganguly, D., P. J. Rasch, H. Wang, and J.-H. Yoon, Climate response of the South Asian
643 monsoon system to anthropogenic aerosols, J. Geophys. Res., 117, D13209,
644 doi:10.1029/2012JD017508, 2012.
645 Garny, H. and Randel, W. J.: Transport pathways from the Asian monsoon anticyclone to the
646 stratosphere, Atmos. Chem. Phys., 16, 2703–2718, doi:10.5194/acp-16-2703-2016,2016.
647 Gautam R., Hsu N. C., Tsay S. C., Lau K. M., Holben B., Bell S., Smirnov A., Li C., Hansell R.,
648 Ji Q., Payra S., Aryal D., Kayastha R., and Kim K. M.: Accumulation of aerosols over the
649 Indo-Gangetic plains and southern slopes of the Himalayas: distribution, properties and
650 radiative effects during the 2009 pre-monsoon season, Atmos. Chem. Phys., 11, 12841–
651 12863, doi:10.5194/acp-11-12841-2011, 2011.
652 Gettelman, A., Forster, P., Fujiwara, M., Fu, Q., Vomel, H., Gohar, L. K., Johanson, C., and
653 Ammerman, M.: Radiation balance of the tropical tropopause layer, J. Geophys. Res.,
654 109, D07103, doi:10.1029/2003JD004190, 2004.
655 Goswami, B. N., V. Krishnamurthy, and H. Annamalai, 1999: A broad scale circulation index for
656 the interannual variability of the Indian summer monsoon. Q. J. R. Meteorol. Soc., 125,
657 pp. 611-633, doi: 10.1002/qj.49712555412, 1999.
658 Govardhan, G., Satheesh, S.K., Nanjundiah,R., Krishna Moorthy, K., and Babu, S. S.: Possible
659 climatic implications of high altitude emissions of black carbon, Atmos. Chem. Phys.
660 Discuss., doi:10.5194/acp-2017-96, 2017.
661 Guelle, W., Schulz, M., Balkanski,Y., Dentener, F.: Influence of the source formulation on
662 modeling the atmospheric global distribution of sea salt aerosol, J. Geophys. Res., 106,
663 27509-27524, doi:10.1029/2001JD900249, 2001.
664 Guenther, A., Hewitt, C. N., Erickson, D., Fall, R., Geron, C., Graedel, T., Harley, P., Klinger,
665 L., Lerdau, M., Mckay, W. A., Pierce, T., Scholes, B., Steinbrecher, R., Tallamraju, R.,
666 Taylor, J., and Zimmerman, P. A.: Global-Model of Natural Volatile Organic-Compound
667 Emissions, J. Geophys. Res.- Atmos., 100, 8873–8892, doi: 10.1029/94JD02950, 1995.
668 Guo L., Highwood E. J., Shaffrey L. C., and Turner A. G.: The effect of regional changes in
669 anthropogenic aerosols on rainfall of the East Asian Summer Monsoon, Atmos. Chem.
670 Phys., 13, 1521-1534, doi:10.5194/acp-13-1521-2013, 2013.

671 Guo, L., Turner. A.G. and Highwood, E. J.: Impacts of 20th century aerosol emissions on the
672 South Asian monsoon in the CMIP5 models, Atmos. Chem. Phys., 15, 6367–6378,
673 doi:10.5194/acp-15-6367-2015, 2015.
678 Haywood, J. M., Shine,K.P.: Multi-spectral calculations of the radiative forcing of tropospheric
679 sulphate and soot aerosols using a column model, Q. J. R. Meteorol. Soc., 123, 1907-
680 1930,doi:10.1002/qj.49712354307, 1997.
681 He, Q. S., Li, C. C., Ma, J. Z., Wang, H. Q., Yan, X. L., Lu, J., Liang, Z. R., and Qi, G. M.:
682 Lidar-observed enhancement of aerosols in the upper troposphere and lower stratosphere
683 over the Tibetan Plateau induced by the Nabro volcano eruption, Atmos. Chem. Phys.,
684 14, 11687-11696, doi:10.5194/acp-14-11687-2014, 2014.
691 Hirose, M., and K. Nakamura, Spatial and diurnal variation of precipitation systems over Asia
692 observed by the TRMM Precipitation Radar, J. Geophys. Res., 110, D05106,
693 doi:10.1029/2004JD004815, 2005.
694 Hodnebrog, O., Myhre,G., Samset, B.H .: How shorter black carbon lifetime alters its climate
695 effect, Nature Communications, 5, doi:10.1038/ncomms6065, 2014.
696 Huffman, G.J., R.F. Adler, D.T. Bolvin, G. Gu, E.J. Nelkin, K.P. Bowman, Y. Hong, E.F.
697 Stocker, D.B. Wolff.: The TRMM Multi-satellite Precipitation Analysis: Quasi-Global,
698 Multi-Year, Combined-Sensor Precipitation Estimates at Fine Scale. J.
699 Hydrometeor., 8(1) ,38-55,doi: http://dx.doi.org/10.1175/jhm560.1, 2007.
700 Jacobson, M. C., Hansson, H.-C., Noone, K. J., and Charlson, R. J.: Organic atmospheric
701 aerosols: Review and state of the science, Rev. Geophys., 38, 267–294,
702 doi: 10.1029/1998RG000045, 2000.
703 Kloster, S., Dentener, F., Feichter, J., Raes, F., Lohmann, U., Roeckner, E., Burns,I.F.: A GCM
704 study of future climate response to aerosol pollution reductions, Clim. Dyn,
705 doi:10.1007/s00382-009-0573-0, 2009.
706 Kopp, R. E., Mauzeralla D. L.: Assessing the climatic benefits of black carbon mitigation,
707 PNAS, 107, 26, 11703-11708, doi: 10.1073/pnas.0909605107, 2010.
708 Krishnamurthy V, Achuthavarier D.: Intraseasonal oscillations of the monsoon circulation over
709 South Asia. Clim. Dyn, 38(11):2335–2353, doi: 10.1007/s00382-011-1153-7, 2012.
710 Kumar, R., Naja, M., Satheesh, S.K., Ojha, N., Joshi, H., Sarangi, T., Pant, P., Dumka, U.C.,
711 Hegde, P., Venkataramani, S.: Influences of the springtime northern Indian biomass

burning over the central Himalayas, J. Geophys. Res., 116, D19302, doi:10.1029/2010JD015509, 2011.

Kummerow, C., Barnes, W., Kozu, T., Shiue, J. and Simpson, J.: The Tropical Rainfall Measuring Mission (TRMM) sensor package. J. Atmos. Oceanic Technol., 15, 809–816, doi: http://dx.doi.org/10.1175/1520-0426(1998)015<0809:TTRMMT>2.0.CO;2, 1998.

Kunze M., Braesicke P., Langematz U., Stiller G., Bekki S, Brühl C., Chipperfield M., Dameris M., Garcia R, and Giorgetta M.:Influences of the Indian Summer Monsoon on Water Vapor and Ozone Concentrations in the UTLS as Simulated by Chemistry–Climate Models, 23, 3525-3544, do1: 10.1175/2010JCLI3280,2010.

Lamarque, J.F., Bond, T.C., Eyring,V., Granier, C., Heil,A., Klimont, A., Lee, D., Liousse,D., Mieville, A., Owen,B., Schultz, M.G., Shindell, D., Smith, S.J., Stehfest,E., Van Aardenne,J., Cooper,O.R., Kainuma, M., Mahowald, N., McConnell, J.R., Naik,V., Riahi, K., van Vuuren, D.P .: Historical (1850–2000) gridded anthropogenic and biomass burning emissions of reactive gases and aerosols: methodology and application, Atmos. Chem. Phys., 10, 7017- 7039, doi:10.5194/acp-10-7017-2010, 2010.

Lau, K. M., Kim, K. M.: Observational relationships between aerosol and Asian monsoon rainfall, and circulation, Geophys. Res. Lett., 33, L21810, doi:10.1029/2006GL027546, 2006.

Lelieveld, J., Crutzen, P. J., Ramanathan, V., Andreae, M. O., Brenninkmeijer, C. A. M., Campos, T., Cass, G. R., Dickerson, R. R., Fischer, H., de Gouw, J. A., Hansel, A., Jefferson, A., Kley, D., de Laat, A. T. J., Lal, S., Lawrence, M. G., Lobert, J. M., Mayol-Bracero, O. L., Mitra, A. P., Novakov, T., Oltmans, S. J., Prather, K. A., Reiner, T., Rodhe, H., Scheeren, H. A., Sikka, D., and Williams, J.: The Indian Ocean Experiment: Widespread Air Pollution from South and Southeast Asia, Science, 291, 1031– 1036,, doi: 10.1126/science.1057103, 2001.

Li, C. and Yanai M.: The onset and interannual variability of the Asian summer monsoon in relation to land–sea thermal contrast, J. Clim. 9: 358–375, doi: http://dx.doi.org/10.1175/1520-0442(1996)009,0358:TOAIVO>2.0.CO;2, 1996.

Li, Q., Jiang, J. H., Wu, D. L., Read, W. G., Livesey, N. J.,. Waters, J.W:, Zhang, Y.,Wang, B., Filipiak, M. J., Davis, C. P., Turquety,S., Wu, S., Park R. J., Yantosca R. M., and Jacob D. J.: Convective outflow of South Asian pollution: A global CTM simulation compared

743 with EOS MLS observations, Geophys. Res. Lett., 32, L14826,
744 doi:10.1029/2005GL022762, 2005.
745 Li, J.-L. F., Walilser, D.E., Chen. W.T., Guan, B., Kubar, T., Stephens, G., Ma, H.Y., Deng, M.,
746 Donner, L., SEman, C., Horowitz, L.: An observationally based evaluation of cloud ice
747 water in CMIP3 and CMIP5 GCMs and contemporary reanalyses using contemporary
748 satellite data, J. Geophys. Res., 117, D16105, doi:10.1029/2012JD017640, 2012.
749 Li, J.-L. F., Waliser, D. E., Stephens, G., Lee, S., L'Ecuyer, T., Kato, S., Loeb, N. and Ma, H.
750 Y.: Characterizing and understanding radiation budget biases in CMIP3/CMIP5 GCMs,
751 contemporary GCM, and reanalysis. J. Geophys. Res., 118, 8166–8184,
752 doi:10.1002/jgrd.50378, 2013.
753 Lin N. H., Tsay, Si-C., Maring, H.B., Yen, M.Ch., Sheu,G.R., Wang, S.H., Chi, K.H., Chuang,
754 M.T., Chang-Feng Ou-Yang , Joshua S. Fu, Jeffrey S. Reid, Chung-Te Lee, Lin-Chi
755 Wang, Jia-Lin Wang , Christina N. Hsu , Andrew M. Sayer, Brent N. Holben, Yu-Chi
756 Chu, Xuan Anh Nguyen, Khajornsak Sopajaree , Shui-Jen Chen, Man-Ting Cheng, Ben-
757 Jei Tsuang, Chuen-Jinn Tsai, Chi-Ming Peng, Russell C. Schnell, Tom Conway, Chang-
758 Tang Chang , Kuen-Song Lin, Ying I. Tsai, Wen-Jhy Lee, Shuenn-Chin Chang, Jyh-Jian
759 Liu, Wei-Li Chiang, Shih-Jen Huang, Tang-Huang Lin, Gin-Rong Liu.: An overview of
760 regional experiments on biomass burning aerosols and related pollutants in Southeast
761 Asia: From BASE-ASIA and the Dongsha Experiment to 7-SEAS, Atmos. Environ., 78,
762 1-19, http://dx.doi.org/10.1016/j.atmosenv.2013.04.066, 2013.
763 Lin C-Y, Zhao C., Liu X., Lin N-H ., ChenW-N.: Modelling of long-range transport of southeast
764 Asia biomass-burning aerosols to Taiwan and their radiative forcings over EAST
765 ASIA,Tellus B 2014, 66, 23733, http://dx.doi.org/10.3402/tellusb.v66.23733, 2014.
766 Liu, H.-L., Wang, P.K., Schlesinger, R.E.: A numerical study of cirrus clouds. Part II: Effects of
767 Ambient Temperature, Stability, Radiation, Ice Microphysics, and Microdynamics on
768 Cirrus Evolution. J. Atmos. Sci. 60, 1097–1119,doi: http://dx.doi.org/10.1175/1520-
769 0469(2003)060<1097:ansocc>2.0.co;2, 2003.
770 Lohmann U., Ferrachat, S.: Impact of parametric uncertainties on the present-day climate and on
771 the anthropogenic aerosol effect, Atmos. Chem. Phys., 10, 11373-11383,
772 doi:10.5194/acp-10-11373-2010, 2010.

773 Lu, Z., Zhang, Q., Streets, D. G.: Sulfur dioxide and primary carbonaceous aerosol emissions in
774 China and India, 1996–2010, Atmos. Chem. Phys., 11, 9839–9864, doi:10.5194/acp-11-
775 9839- 2011, 2011.
776 Manoj M. G., Devara, P.C.S., Safai, P.D., Goswami, B.N.: Absorbing aerosols facilitate
777 transition of Indian monsoon breaks to active spells, Clim. Dyn, 37:2181–2198, doi:
778 10.1007/s00382-010-0971-3, 2011.
779 Meehl, G. A.: Coupled land-ocean-atmosphere processes and South Asian monsoon variability,
780 Science, 266, 263–267, doi: 10.1126/science.266.5183.263, 1994.
781 Meehl G A, Arblaster J.M., Collins, W.D.: Effects of black carbon aerosols on the Indian
782 monsoon, J. Climate, 21, 2869–2882, doi: http://dx.doi.org/10.1175/2007JCLI1777.1,
783 2008.
784 Menon, S., Hansen, J., Nazarenko, L., and Luo, Y.: Climate Effects of Black Carbon Aerosols in
785 China and India, Science, 297, 2250–2253, doi: 10.1126/science.1075159, 2002.
786 Mieville, A., C. Granier, C. Liousse, B. Guillaume, F. Mouillot, J.F. Lamarque, J.M. Gregoire,
787 and G. Petron.: Emissions of gases and particles from biomass burning using satellite
788 data and an historical reconstruction, Atmos. Environ., 44, 1469–1477,
789 doi:10.1016/j.atmosenv.2010.01.011, 2010.
790 Myhre, G., Shindell, D., Bréon, F. M., Collins, W., Fuglestvedt, J., Huang, J., Koch, D.,
791 Lamarque, J.-F., Lee, D., Mendoza, B., Nakajima, T., Robock, A., Stephens, G. ,
792 Takemura T. and Zhang, H., Anthropogenic and Natural Radiative Forcing. In: Climate
793 Change 2013: The Physical Science Basis. Contribution of Working Group I to the Fifth
794 Assessment Report of the Intergovernmental Panel on Climate Change [Stocker, T.F., D.
795 Qin, G.-K. Plattner, M. Tignor, S.K. Allen, J. Boschung, A. Nauels, Y. Xia, V. Bex and
796 P.M. Midgley (eds.)]. Cambridge University Press, Cambridge, United Kingdom and
797 New York, NY, USA., 2013.
798 Neubauer D., Lohmann U. and Hoose C. and Frontoso, M. G.: Impact of the representation of
799 marine stratocumulus clouds on the anthropogenic aerosol effect Atmos. Chem. Phys.,
800 14, 11997–12022, doi:10.5194/acp-14-11997-2014, 2014.
801 Pan X., Chin M., Gautam R., Bian H., Kim D., Colarco P. R., Diehl T. L., Takemura T., Pozzoli
802 L., Tsigaridis K., Bauer S., and Bellouin N., A multi-model evaluation of aerosols over

South Asia: common problems and possible causes, Atmos. Chem. Phys., 15, 5903–5928, doi:10.5194/acp-15-5903-2015, 2015.

Park, M., Randel,W.J., Gettelman, A., Massie, S.T., Jiang, J.H.:Transport above the Asian summer monsoon anticyclone inferred from Aura Microwave Limb Sounder tracers, J. Geophys. Res., 112, D16309, doi:10.1029/2006JD008294, 2007.

Park, M., Randel, W.J., Emmons, L.K., Bernath, P.F., Walker, K.A., Boone, C.D.: Chemical isolation in the Asian monsoon anticyclone observed in Atmospheric Chemistry Experiment (ACE-FTS) data, Atmos. Chem. Phys.,doi:10.5194/acp-8-757-2008,2008.

Park, M., Randel, W. J., Emmons, L. K., Livesey, N. J.: Transport pathways of carbon monoxide in the Asian summer monsoon diagnosed from Model of Ozone and Related Tracers (MOZART), J. Geophys. Res., 114, D08303, doi:10.1029/2008JD010621, 2009.

Penner, J. E., Chuang, C.C., Grant, K.: Climate forcing by carbonaceous and sulfate aerosols, Clim. Dyn., 14, 839 -851, doi:10.1007/s003820050259, 1998.

Ploeger, F., Fueglistaler, S., Grooß, J.-U., Günther, G., Konopka, P., Liu, Y. S., Müller, R., Ravegnani, F., Schiller, C., Ulanovski, A., and Riese, M.: Insight from ozone and water vapour on transport in the tropical tropopause layer (TTL), Atmos. Chem. Phys., 11, 407-419, doi:10.5194/acp-11- 407-2011, 2011.

Ploeger F., Konopka P., Müller R., Fueglistaler S., Schmidt T., Manners J., Grooss J.-U., Günther G., de Forster P.M., and Riese M., Horizontal transport affecting trace gas seasonality in the tropical tropopause layer TTL, J. Geophys. Res., 117, D09303,doi:10.1029/2011JD017267, 2012.

Ploeger, F., G. Günther, P. Konopka, S. Fueglistaler, R. Müller, C. Hoppe, A. Kunz, R. Spang, J.-U. Grooß, and M.Riese , Horizontal water vapor transport in the lower stratosphere from subtropics to high latitudes during boreal summer, J. Geophys. Res. Atmos., 118, 8111–8127, doi:10.1002/jgrd.50636, 2013.

Powell K., Vaughan M., Winker D.,K. M. Lee, Pitts M., Trepte C.: CALIPSO Data Product Catalog,Release 3.6, Document No: PC-SCI-503, 2013.

Rahul P. R. C., Bhawar R. L., Ayantika D. C., Panicker A. S., Safai P. D., Tharaprabhakaran V., Padmakumari B., and Raju M. P., Double blanket effect caused by two layers of black carbon aerosols escalates warming in the Brahmaputra River Valley, Scientific Reports, 4, 3670, DOI: 10.1038/srep03670, 2014.

840 Rajagopalan, B., and P. Molnar, Signatures of Tibetan Plateau heating on Indian summer
841 monsoonrainfall variability, J. Geophys. Res. Atmos., 118, 1170–1178,
842 doi:10.1002/jgrd.50124, 2013.
843 Ramanathan, V., Crutzen, P. J., Lelieveld, J., Mitra, A. P., Althausen,D., Anderson, J., Andreae,
844 M. O., Cantrell, W., Cass,G. R., Chung, C. E., Clarke, A. D., Coakley, J. A., Collins,W.
845 D.,Conant, W. C., Dulac, F., Heintzenberg, J., Heymsfield, A. J.,Holben, B., Howell, S.,
846 Hudson, J., Jayaraman, A., Kiehl, J. T.,Krishnamurti, T. N., Lubin, D., McFarquhar, G.,
847 Novakov, T.,Ogren, J. A., Podgorny, I. A., Prather, K., Priestley, K., Prospero,J. M.,
848 Quinn, P. K., Rajeev, K., Rasch, P., Rupert, S., Sadourny,R., Satheesh, S. K., Shaw, G.
849 E., Sheridan, P., and Valero, F. P. J.: Indian Ocean Experiment: An integrated analysis of
850 the climateforcing and effects of the great Indio-Asian haze, J. Geophys.Res., 106,
851 28371–28398, 2001.
852 Ramanathan, V., Crutzen, P. J., Kiehl, J. T. and Rosenfeld, D., Aerosols, Climate, and the
853 Hydrological Cycle , Science 294**,** 2119–2124, doi: 10.1126/science.1064034, 2001b.
854 Ramanathan V. Crutzen P. J.: New directions: Atmospheric brown “clouds”, Atmos.
855 Environ. 37:4033–4035, doi:10.1016/S1352-2310(03)00536-3, 2003.
856 Ramanathan, V. and Carmichael, G.: Global and regional climate changes due to black carbon,
857 Nat. Geosci., 1, 221–227, doi:10.1038/ngeo156, 2008.
858 Ramaswamy, V., Ramanathan, V. Solar absorption of cirrus clouds and the maintenance of the
859 tropical upper troposphere thermal structure. J. Atmos. Sci. 46, 2293–2310, doi:
860 http://dx.doi.org/10.1175/1520-0469(1989)046<2293:SABCCA>2.0.CO;2 1989.
861 Randall, D.A., Harshovardan, Dazlich, D.A., Corsetti, T.G. Interactions among radiation,
862 convection, and large-scale dynamics in a general circulation model. J. Atmos. Sci. 46,
863 1943–1970, doi:10.1175/1520-0469(1989)046<1943:IARCAL>2.0.CO;2, 1989.
864 Randel,W. J. and Park, M.: Deep convective influence on the Asian summer monsoon
865 anticyclone and associated tracer variability observed with Atmospheric Infrared Sounder
866 (AIRS), J. Geophys. Res., 111, D12314, doi:10.1029/2005JD006490, 2006.
867 Randel, W. J., Park, M., Emmons, L., Kinnison, D., Bernath, P., Walker, K. A., Boone, C., and
868 Pumphrey H.: Asian monsoon transport of pollution to the stratosphere, Science, 328,
869 611–613, doi: 10.1126/science.1182274, 2010.

870 Rosenfield, D., Suppression of rain and snow by urban and industrial air pollution, Science, 287,
871 1793–1796, doi: 10.1126/science.287.5459.1793, 2000.
872 Satheesh, S. K. and Ramanathan, V.: Large differences in tropical aerosol forcing at the top of
873 the atmosphere and Earth's surface, Nature, 405, 60–63, doi:10.1038/35011039, 2000.
874 Schultz, M. G., Heil, A., Hoelzemann, J. J., Spessa, A., Thonicke, K., Goldammer, J., Held, A.
875 C., Pereira, J. M., and van het Bolscher, M.: Global wildland fire emissions from 1960 to
876 2000, Global Biogeochem. Cyc., 22, GB2002, doi:10.1029/2007GB003031, 2008.
877 Solomon, S., Qin, D., Manning, M., Chen, Z., Marquis, M., Averyt, K.B., Tignor M. and Miller,
878 H. L., Contribution of Working Group I to the Fourth Assessment Report of the
879 Intergovernmental Panel on Climate Change,Cambridge University Press, Cambridge,
880 United Kingdom and New York, NY, USA. 2007.
881 Sreekanth, V., Niranjan, K. and Madhavan , B. L., Radiative forcing of black carbon over eastern
882 India, Geophys. Res. Lett., 34, L17818, doi:10.1029/2007GL030377, 2007.
883 Stephens, G. L., Vane, D.G., Taneeli, S., Im,E., Durden, S., Rockey, M., Reinke, D., Partain, P.,
884 Mace, G.G., Austin, R., Ecuyet, T.L., Haynes, J., Lebsock, M., Suzuki, K., Waliser, D.,
885 Wu, D., Kay, J., Gettelman, A., Wang, Z., Marchand, R.: CloudSat mission: Performance
886 and early science after the first year of operation, J. Geophys. Res., 113, D00A18,
887 doi:10.1029/2008JD009982,2008.
888 Stevens, B., Giorgetta M., Esch M., Mauritsen T., Crueger T., Rast S., Salzmann M., Schmidt H.,
889 Bader J., Block K., Brokopf R., Fast I., Kinne S., Kornblueh L., Lohmann U., Pincus R.,
890 Reichler T., and Roeckne E., Atmospheric component of the MPI-M Earth System
891 Model: ECHAM6, J. of Advances in Modeling Earth Systems. **5**, 1–27,
892 doi:10.1002/jame.20015, 2013.
893 Stier, P., Feichter, J., Kinne, S., Kloster, S., Vignati, E., Wilson, J., Ganzeveld, L., Tegen, I.,
894 Werner, M., Balkanski, Y., Schulz, M., Boucher, O., Minikin, A. and Petzold, A.,:The
895 aerosol-climate model ECHAM5-HAM, Atmos. Chem. Phys., **5**, 1125-1156,
896 doi:10.5194/acp-5-1125-2005, 2005.
897 Streets, D. G., Yan, F., Chin, M., Diehl, T., Mahowald, N., Schultz, M., Wild, M., Wu, Y., and
898 Yu, C.: Anthropogenic and natural contributions to regional trends in aerosol optical
899 depth, 1980–2006, J. Geophys. Res., 114, D00D18, doi:10.1029/2008jd011624, 2009.

Takahashi, H. G.: Seasonal and diurnal variations in rainfall characteristics over the tropical Asian monsoon region using TRMM-PR data. SOLA, 12A, 22−27, doi:10.2151/sola.12A-005, 2016.

Tegen, I., Harrison, S. P., Kohfeld, K., Prentice, I. C., Coe, M., and Heimann, M.: Impact of vegetation and preferential source areas on global dust aerosol: Results from a model study, J. Geophys. Res.-Atmos., 107, 4576, doi:10.1029/2001JD000963, 2002.

Thomason, L. W. and Vernier, J.P.: Improved SAGE II cloud/aerosol categorization and observations of the Asian tropopause aerosol layer: 1989–2005, Atmos. Chem. Phys., 13, 4605-4616, doi:10.5194/acp-13-4605-2013, 2013.

Tobo, Y., Iwasaka, Y., Yu Shi, G.,Kim, Y. S., Ohashi, T, Tamura, K. and Zhang, D.:Balloon-borne observations of high aerosol concentrations near the summertime tropopause over the Tibetan Plateau, Atmospheric Research,84, 233–241,doi:10.1016/j.atmosres.2006.08.003, 2007.

Tripathi, S.N., Srivastava, A.K., S. Dey, S., Satheesh, S.K., Krishnamoorthy,K.: The vertical profile of atmospheric heating rate of black carbonaerosols at Kanpur in northern India, Atmos. Environ., 41,6909–6915, doi: http://dx.doi.org/10.1016/j.atmosenv.2007.06.032, 2007.

Van derWerf, G. R., Randerson, J.T., Giglio, L., Collatz, G.J., Kasibhatla, P.S., Arellano A.F.: Interannual variability in global biomass burning emissions from 1997 to 2004, Atmos. Chem. Phys., **6**, 3423-3441, doi:10.5194/acp-6-3423-2006, 2006.

Vernier, J. P., L. W. Thomason, and J. Kar.: CALIPSO detection of an Asian tropopause aerosol layer, Geophys. Res. Lett., 38, L07804, doi:10.1029/2010GL046614, 2011.

Vernier, J.P., Fairlie, T.D., Natarajan, M., Wienhold, F.G., Bian, J., Martinsson, B.G., Crumeyrolle, S., Thomason, L.W., Bedka, K.M.: Increase in upper tropospheric and lower stratospheric aerosol levels and its potential connection with Asian pollution, J. Geophys. Res. Atmos., 120, 1608–1619, doi:10.1002/2014JD022372, 2015.

Vignati, E., Wilson,J., and Stier,P.: An efficient size-resolved aerosol microphysics module for large-scale aerosol transport models, J. Geophys. Res.,109, D22202, doi:10.1029/2003JD004485, 2004.

933 Vinoj V, Rasch P. J., Wang H., Yoon J-H, Ma P-L, Landu K. and Singh B., Short-term
934 modulation of Indian summer monsoon rainfall by West Asian dust, Nature Geoscience
935 7, 308–313, doi:10.1038/ngeo2107, 2014.
936 Vogel B., Pan L. L., Konopka P., Günther G., Müller R., Hall W., Campos T., Pollack T.,
937 Weinheimer A., Wei J., Atlas E. L. and Bowman K.P., Transport pathways and
938 signatures of mixing in the extratropical tropopause region derivedfrom Lagrangian
939 model simulations, J. Geophys. Res., 116, D05306, doi:10.1029/2010JD014876, 2011.
940 Vogel B., Günther G., Müller R., Grooß J.-U., and Riese M., Impact of different Asian source
941 regions on the composition of the Asian monsoon anticyclone and of the extratropical
942 lowermost stratosphere, Atmos. Chem. Phys., 15, 13699–13716, doi:10.5194/acp-15-
943 13699-2015, 2015.
944 Wang, B. and Linho, Rainy Season of the Asian–Pacific Summer Monsoon, Journal of Climate,
945 15, 386-398, http://dx.doi.org/10.1175/1520-0442(2002)015<0386:RSOTAP>2.0.CO;2
946 2002.
947 Wang, C. A modeling study on the climate impacts of black carbon aerosols, J. Geophys. Res.,
948 109, D03106, doi:10.1029/2003JD004084, 2004.
949 Wang, C., Impact of direct radiative forcing of black carbon aerosols on tropical convective
950 precipitation, Geophys. Res. Lett., 34, L05709, doi:10.1029/2006GL028416, 2007.
951 Wang, C., Kim, D., Ekman, A. M. L.,. Barth, M. C and Rasch, P. J.: Impact of anthropogenic
952 aerosols on Indian summer monsoon, Geophys. Res. Lett., 36, L21704,
953 doi:10.1029/2009GL040114, 2009.
954 Winiger P., Andersson A., Eckhardt S., Stohl A. and Gustafsson O.:The sources of atmospheric
955 black carbon at a European gateway to the Arctic, Nature Communications, 7, 12776,
956 doi: 10.1038/ncomms12776, 2016.
957 Winker, D., Pelon, J., Coakley, J., Ackerman, S., Charlson, R., Colarco, P., Flamant, P., Fu, Q.,
958 Hoff, R., Kittaka, C., Kubar, T.L., Le Treut, H., McCormick, M.P., Mégie,G., Poole,L.,
959 Powell, K., Trepte, C., Vaughan, M.A., Wielicki, B.A.:THE CALIPSO MISSION A
960 Global 3D View of Aerosols and Clouds. Bull Amer Meteorol Soc.,91, 1211-1229, doi:
961 http://dx.doi.org/10.1175/2010bams3009.1,2010.

962 Wu G., and Zhang Y. : Tibetan Plateau forcing and timing of the monsoon onset over South Asia
963 and South China Sea, Monthly Weather Review, 126, 913–927, doi:
964 http://dx.doi.org/10.1175/1520-0493(1998)126<0913:tpfatt>2.0.co;2, 1998.
965 Xie, P., Yatagai,A., Chen, M., Hayasaka, T., Fukushima, Y., Liu, C., Yang, S.: A Gauge-
966 Based Analysis of Daily Precipitation over East Asia,Journal of Hydrometeorology, doi:
967 10.1175/JHM583.1, 2007.
968 Xiong, X., Houweling, S., Wei, J., Maddy, E., Sun, F., and Barnet, C.: Methane plume over
969 south Asia during the monsoon season: satellite observation and model simulation,
970 Atmos. Chem. Phys., 9, 783–794, doi:10.5194/acp-9-783-2009, 2009.
971 Yanai, M., Li, C., Song, Z.: Seasonal heating of the Tibetan Plateau and its effects on the
972 evolution of the Asian summer monsoon, J Meteor Soc Japan, 70, 189–221, 1992.
973 Yu, P., Toon, O.B., Neely, R.R., Martinsson, B.G., Brenninkmeijer, C.A.M.: Composition and
974 physical properties of the Asian Tropopause Aerosol Layer and the North American
975 Tropospheric Aerosol Layer, Geophys. Res. Lett., 42, 2540–2546, doi:10.1002/, 2015.
976 Zhang K., D. O'Donnell, J. Kazil, P. Stier, S. Kinne, U. Lohmann, S. Ferrachat, B. Croft, J.
977 Quaas, H, Wan, S. Rast, and J. Feichter 2012.: The global aerosol-climate model
978 ECHAM-HAM, Version 2: Sensitivity to improvements in process representations,
979 Atmos. Chem. Phys., **12**, 8911-8949, doi:10.5194/acp-12-8911-2012, 2012.
980 Zhang L., Henze D. K., Grell G. A., Carmichael G. R., Bousserez N., Zhang Q., Torres O., Ahn
981 C., Lu Z., Cao J., and Mao Y.: Constraining black carbon aerosol over Asia using OMI
982 aerosol absorption optical depth and the adjoint of GEOS-Chem, Atmos. Chem. Phys.,
983 15, 10281–10308, doi:10.5194/acp-15-10281-2015, 2015.
984

Table-1: ECHAM6 HAM simulated total (shortwave and long wave) radiative forcing (W m^{-2}) averaged over the ASM region.

Model run	TOA	Surface	Atmosphere
Demiss-CTRL	+0.37	-4.74	+5.11
DBConly-CTRL	+0.31	-4.20	+4.52
DOConly-CTRL	-0.51	-1.96	+1.45

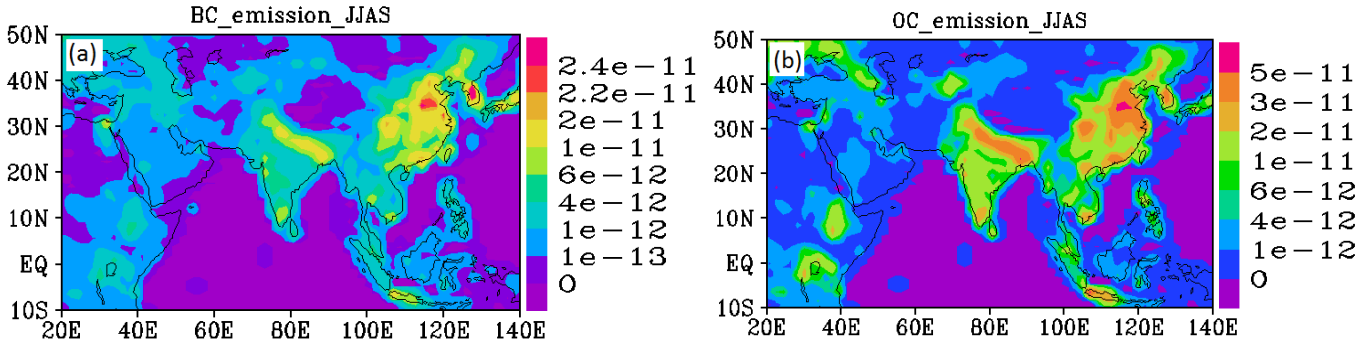

Figure1: Distribution of emission mass flux (kg m^{-2} s^{-1}) averaged for the monsoon season (June-September) for **(a)** BC and **(b)** OC aerosols.

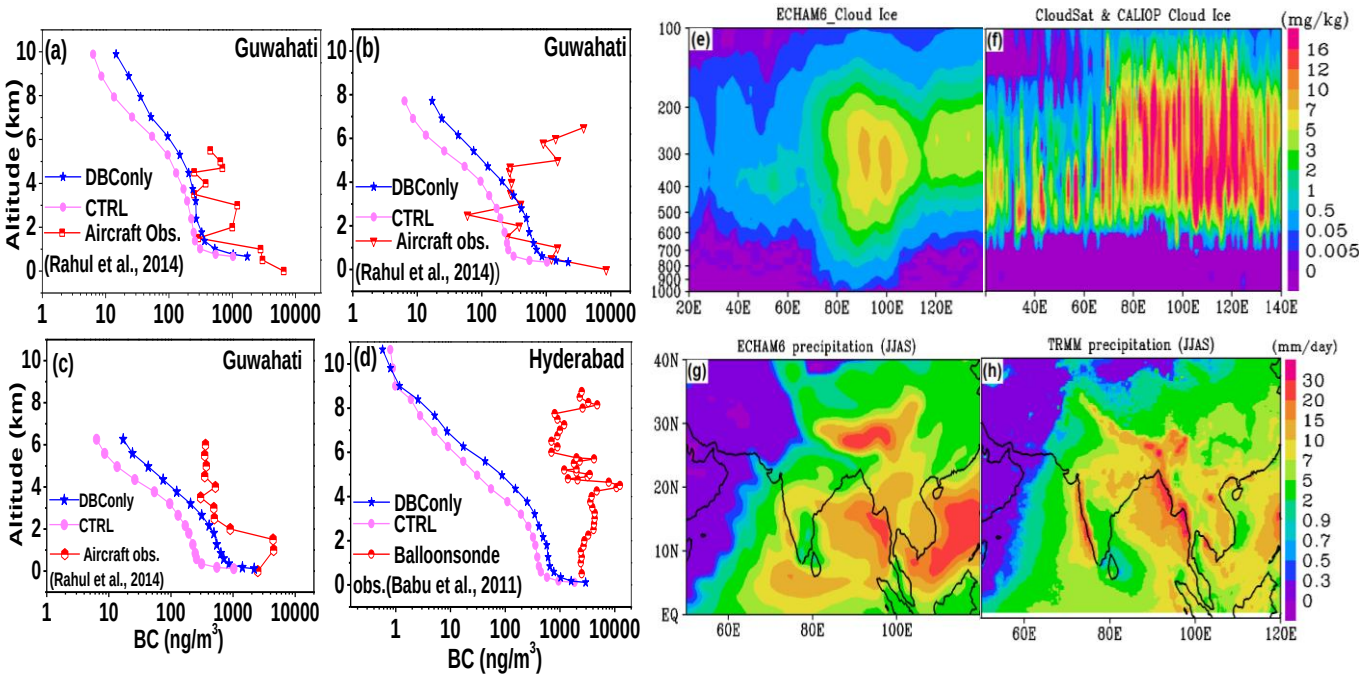

Figure 2: Vertical distribution of BC aerosols (ng m^{-3}) (a) aircraft measurements on 30 August 2009 at Guwahati (26°11′N, 91°44′E) (Rahul et al., 2014), CTRL, DBConly simulations for the month of August extracted at a grid centered at Guwahati, (b) same as (a) but observations for 4 September 2009 and simulations for the month of September, (c) same as (a) but for observations on 6 September 2009 and simulations for the month of September, (d) Balloonborne measurement on 17 March 2010 at Hyderabad (17.48 °N,78.40° E) (Babu et al., 2011) and CTRL, DBConly simulations for the month of March at a grid centred at Hyderabad. Seasonal mean distribution of cloud ice mass mixing ratio (mg kg^{-1}) averaged for 20°N-40°N (e) CTRL simulation (f) CloudSat and CALIPSO combined 2C-ICE L3 for the years 2007-2010. Seasonal mean precipitation (mm day^{-1}) obtained from (g) CTRL simulation (h) TRMM averaged for period 1998-2005.

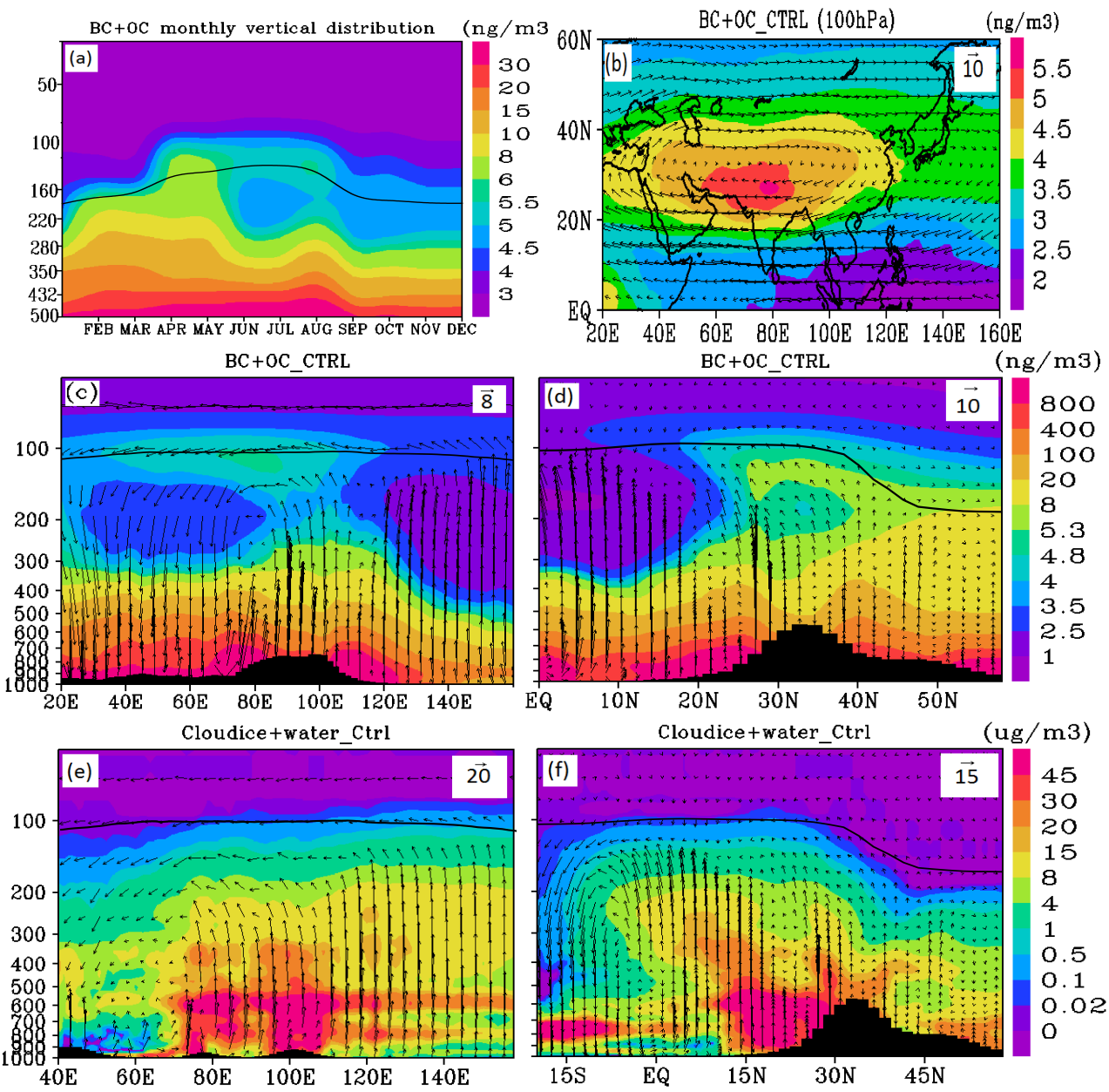

Figure 3: Distribution of BC and OC aerosols (ng m^{-3}) together (a) monthly variations averaged for the region 70°E - 120°E, 25°E - 45°E, Seasonal mean distribution of BC and OC aerosols (ng m^{-3}) together (b) at 100 hPa, (c) averaged for 15°N - 35°N, (d) averaged for 80°E - 110°E, seasonal mean distribution of cloud ice+cloud water (µg m^{-3}) (e) averaged for 10°N - 25°N, (f) averaged for 80°E - 110°E. Black arrows indicate wind vectors. The vertical velocity field has been scaled by 1000. The black line represents the tropopause. In Figs. (a), (c), (d), (e), (f) tropopause is averaged over the same region where field parameter is averaged.

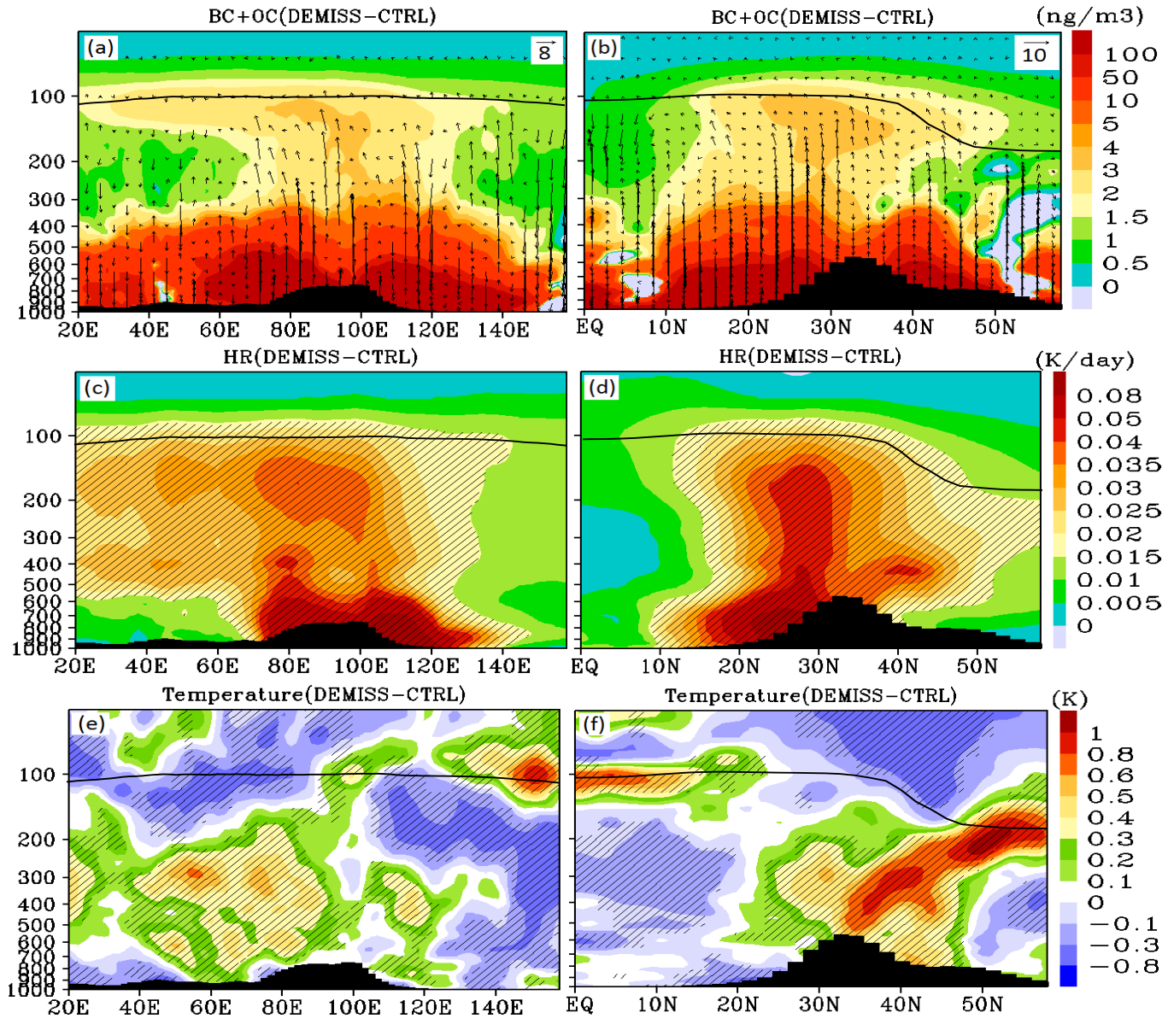

Figure 4: Distribution of anomalies (Demiss - CRTL), of BC and OC aerosols (ng m^{-3}) together averaged for the monsoon season (a) averaged for 15°N -35°N (b) averaged for 80ºE-110°E, Black arrows indicate wind vectors (the vertical velocity field has been scaled by 1000), (c) and (d) same as (a) and (b) but for heating rate anomalies (K/day). Distribution of anomalies in temperature (K) (e) averaged for 15ºN-35°N, (f) averaged for 80°E -110°E. The black line represents the tropopause. The tropopause is averaged over 15°N -35°N for Figs. (a), (c) , (e) and over 80ºE-110°E for Figs. (b), (d) and (f). Black hatched lines in Figs.(c), (d), (e) and (f) indicate 99% confidence level.

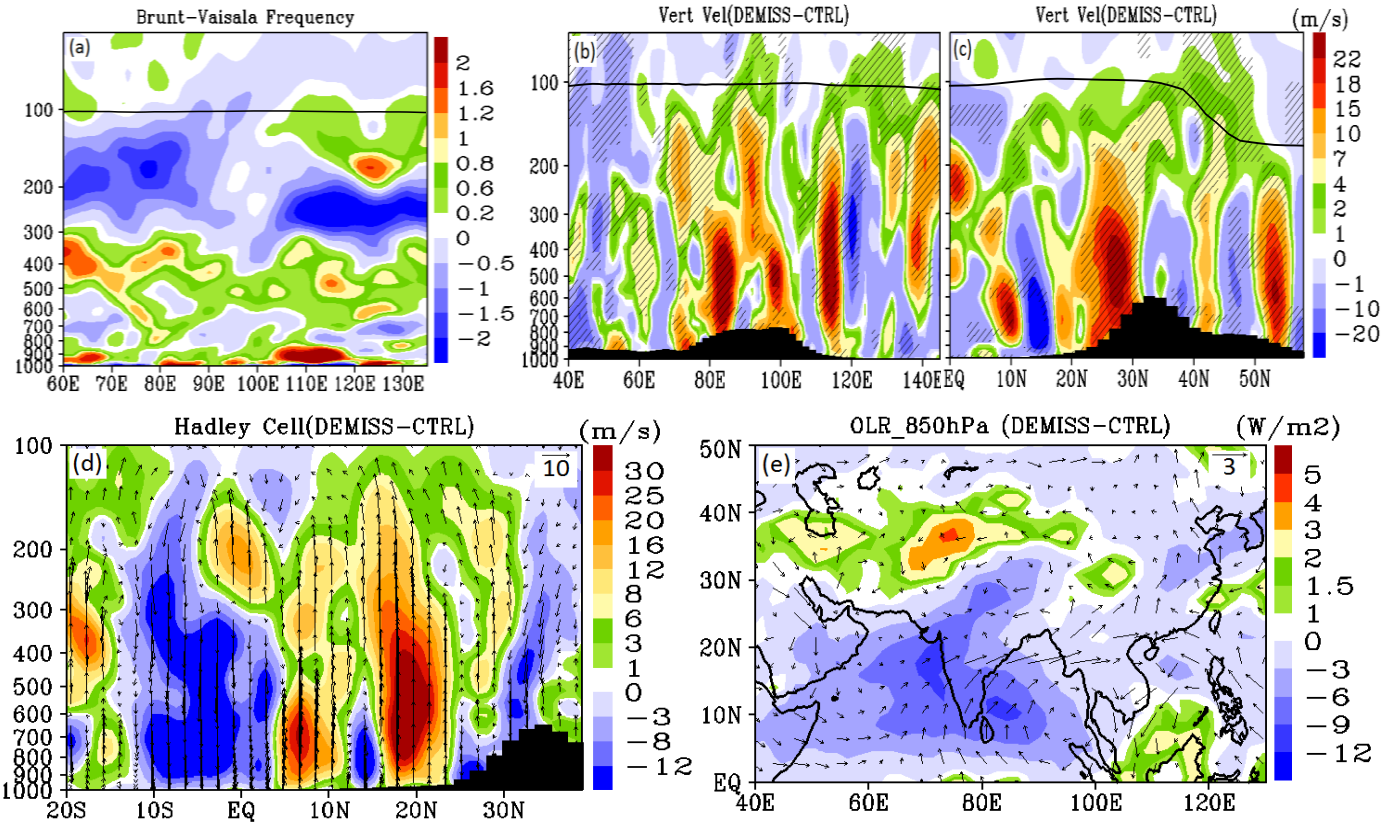

Figure 5: Vertical distribution of anomalies (Demiss-CTRL) averaged for the monsoon season (a) square of Brunt Väisälä frequency (per sec*1E-5) averaged over 25°N-40°N, (b) vertical velocities (m s^{-1}) averaged for 15ºN - 35°N, (c) same as (b) but averaged for 80ºE-110°E, (d) difference in the meridional circulation averaged for 70ºE-90ºE. Black arrows indicate wind vectors, (e) Distribution of OLR (shaded) (W/m^2) and winds at 850 hPa (m s^{-1}). In Figs (b)-(d) the vertical velocity field has been scaled by 1000 and the thick black line shows the tropopause. Black hatched lines in Figs (b) and (c) indicate 99% confidence level.

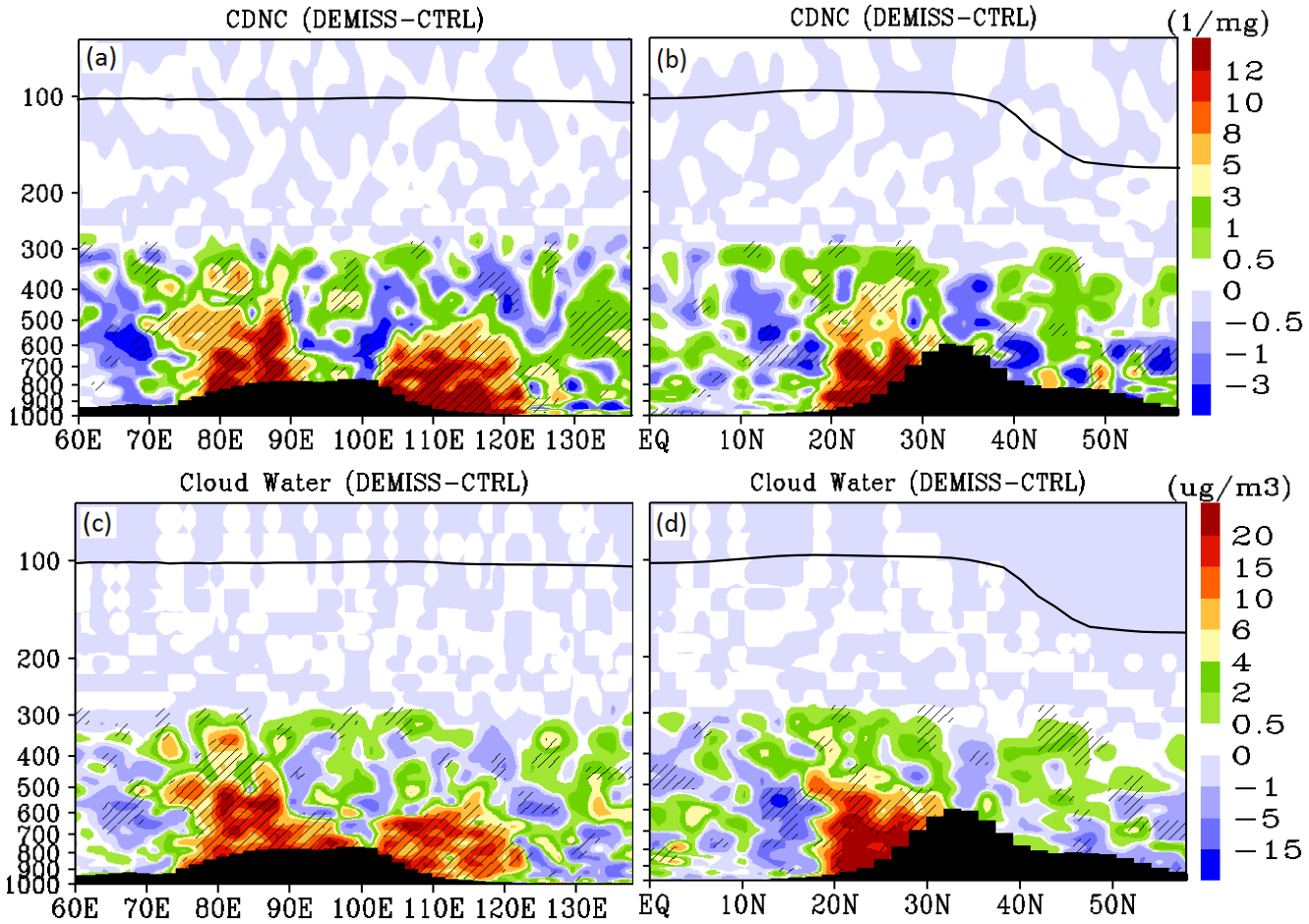

Figure 6: Distribution of anomalies (Demiss-CTRL) averaged for the monsoon season (a) CDNC (mg^{-1}) averaged for 15°N-35°N, (b) same as (a) but averaged for 80°E-110°E, (c) cloud water (µg m^{-3}) averaged for 15°N-35°N, (d) same as (c) but averaged over 80°E-110°E. Black hatched lines in Figs. a-d indicate 99% confidence level.

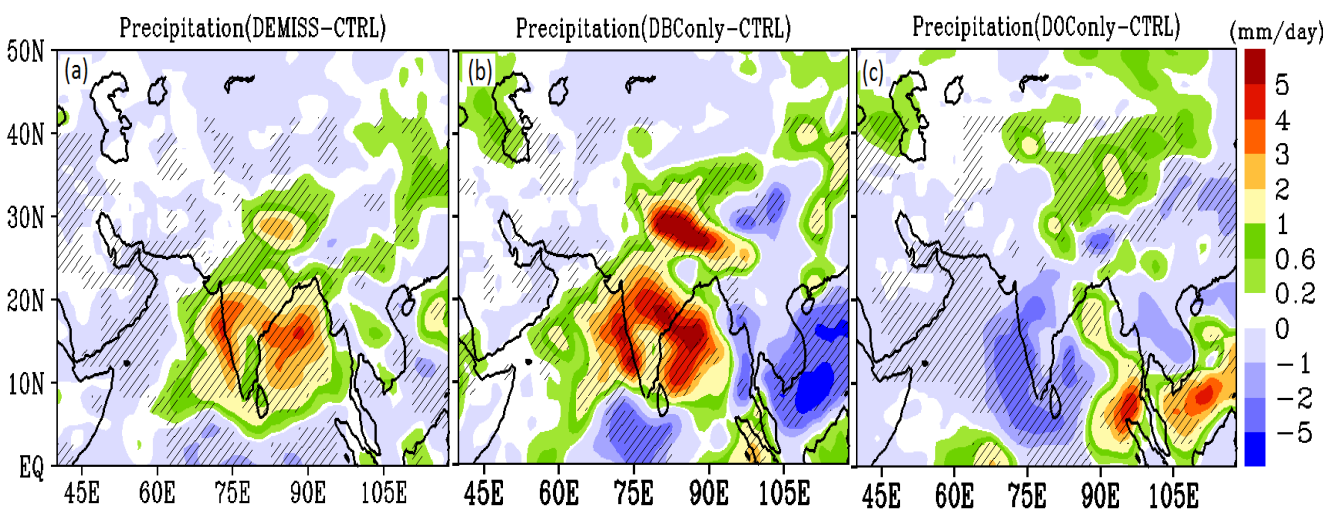

Figure 7: Distribution of anomalies in precipitation (mm day^{-1}) averaged for the monsoon season obtained from (a) Demiss-CTRL, (b) DBConly-CTRL, (C) DOConly-CTRL. Black hatched lines indicate 99% confidence level.

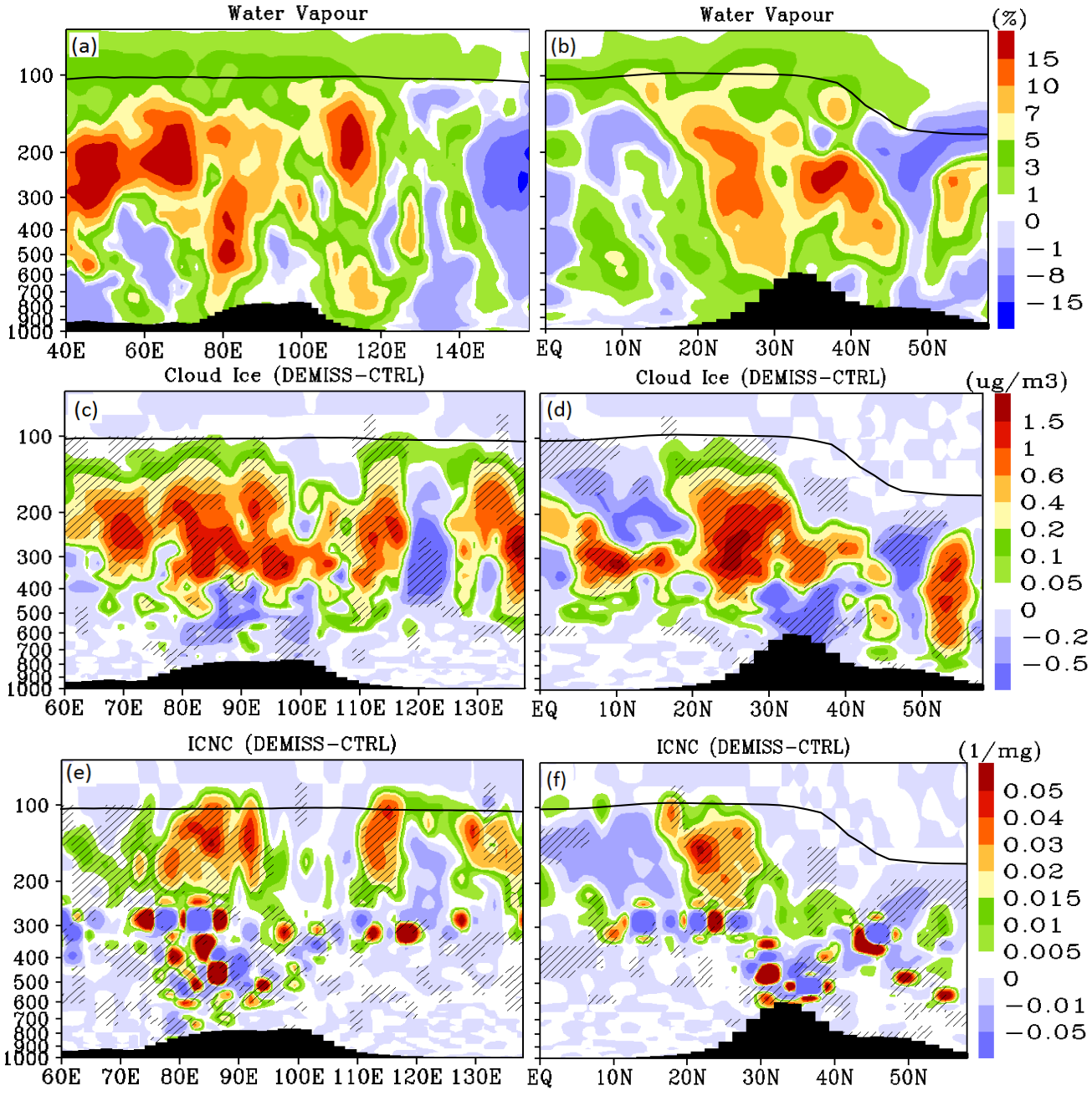

Figure 8: Distribution of anomalies (Demiss-CTRL) averaged for the monsoon season, (a) water vapour (%) averaged over 15°N - 35°N, (b) same as (a) but averged over 80°E - 110°E, (c) and (d) same as (a) and (b) but for cloud ice (µg m^{-3}) and (e) and (f) for ice crystal number concentration (ICNC) (mg^{-1}). The thick black line shows the tropopause while black hatched lines indicate 99% confidence level. The tropopause is averaged over 15°N -35°N for Figs. (a), (c), (e) and over 80ºE-110°E for Figs. (b), (d) and (f). Black hatched lines indicate 99% confidence level.